Ore Geology Reviews 86 (2017) 867–895

Contents lists available at ScienceDirect

Ore Geology Reviews

journal homepage: www.elsevier.com/locate/oregeorev

Magmato-hydrothermal space: A new metric for geochemical characterisation of metallic ore deposits

Carl W. Brauhart [a,*], Eric C. Grunsky [b], Steffen G. Hagemann [a]

[a] Centre for Exploration Targeting, University of Western Australia, 35 Stirling Highway Crawley, Perth, Western Australia 6009, Australia
[b] Department of Earth and Environmental Sciences, University of Waterloo, Waterloo, N2L 3G1, Canada

ARTICLE INFO

Article history:
Received 28 January 2016
Accepted 1 November 2016
Available online 4 Novermber 2016

ABSTRACT

"Magmato-Hydrothermal Space" is a new mathematical construct where 24 ore and pathfinder elements are used to quantify ore-element signatures. Quantification allows relationships between ore deposit samples to be mapped. The broad-scale view of Magmato-Hydrothermal Space reveals three important trends: (1) Zn-Pb sediment-hosted mineralisation to igneous-associated Cu-Au mineralisation, (2) Cu-Au mineralisation to Au-only mineralisation, and (3) ultramafic associated magmatic Ni-Cu-PGE mineralisation through Cu-Au mineralisation to granitoid-associated Mo, W and Sn mineralisation. The view provided by Magmato-Hydrothermal Space reveals that there is a spectrum of ore element signatures that mirrors the spectrum of ore deposit classes described in the literature.

Geochemical variations within individual ore deposit classes are examined for orogenic-Au, VHMS, epithermal and sediment-hosted Cu samples. Sub-groups within each of these classes are compared on element enrichment diagrams and described in the context of Magmato-Hydrothermal Space. Orogenic Au samples are divided into two sub-groups of As-Sb rich mineralisation and four sub-groups of relatively As-Sb poor mineralisation. The As-Sb poor sub-groups include a Te-Cu-Ag rich sub-group that overlaps with the porphyry Cu class and a Te-W-(Bi-Mo) rich class dominated by granitoid hosted deposits. The VHMS class ranges from a Cu-rich sub-group that overlaps with porphyry Cu and IOCG classes through a Cu-Zn sub-group to two Zn-Cu sub-groups, one of which overlaps with the SHMS class. The epithermal class is divided into Zn-rich, Cu-rich and base metal – poor sub-groups.

1. Introduction

It has long been recognised that different metal enrichments characterise different mineral deposit classes (e.g., Lindgren, 1913). Modern geochemical techniques (e.g., Longerich et al., 1990) accurately quantify most ore and pathfinder element concentrations down to, or in many cases well below, average crustal abundance. There are numerous descriptions in the literature of ore deposit geochemistry covering a very wide range of hydrothermal and magmatic ores (e.g., Hedenquist et al., 2005). If metal associations are described with sufficient clarity, that information alone serves as a "fingerprint" or "signature" by which the style of mineralisation can be tightly constrained.

Metal associations are recognised through quantitative assay data, but are normally described in a qualitative list format; e.g., Mortensen et al. (2010) describe Au-As-W-Cu-Pb-Zn enrichment for the Macraes orogenic-Au deposit in New Zealand. Elements listed depend upon the assay suite, detection limits, and those elements the author judges to be significant enough to warrant inclusion. Only subjective means of comparison are available such as "very similar", "somewhat similar", "unrelated" or "completely different". For example, a Zn-Pb-Ag-As-Tl-Sb enriched sample from a Shale Hosted Massive Sulphide (SHMS) deposit has a *similar* signature to a Pb-Zn-Ag-Cd rich sample of Mississippi Valley Type (MVT) ore, but *quite different* to a Zn-Cu-Ag-Au-Bi-Sn rich sample from a Volcanic Hosted Massive Sulphide (VHMS) deposit and *very different* to a sample of Fe-Cu-Au-La-U-Ag-Te-Bi ore from an Iron Oxide Copper Gold (IOCG) deposit. Thus, a quantitative framework in which similarities between ore-element signatures can be measured is an attractive proposition.

"Magmato-Hydrothermal Space" (MH-Space) is a method to quantitatively describe the full range of ore deposit geochemistry. It is a mathematical construct which, in this paper, discriminates ore-signatures with 24 ore and pathfinder elements: Fe, Co, Ni, Re, Pd, Pt, Cu, Ag, Au, Zn, Cd, In, Pb, Tl, Hg, As, Sb, Bi, Te, Mo, W, Sn, La, U. These elements

* Corresponding author at: CSA Global, 2/3 Ord Street, West Perth, Western Australia 6005, Australia.
E-mail address: carl.brauhart@uwa.edu.au (C.W. Brauhart).

http://dx.doi.org/10.1016/j.oregeorev.2016.11.001
0169-1368/

have been selected to characterise metal enrichment patterns in most classes of metallic ore deposit, but the technique can be adapted for a greater or lesser number of variables as required.

2. OSNACA transform

A new mathematical transform has been developed to calculate coordinates in MH-Space. The OSNACA (Ore Samples Normalised to Average Crustal Abundance) transform scales data after log normalising to average crustal abundance.

The OSNACA transform has four steps:

1. replace data below average crustal abundance (ACA) with ACA, or half the limit of detection, whichever is higher,
2. normalise to ACA or half the limit of detection, whichever is higher,
3. transform by $\log_{10}$ for elements with ACA <1 ppm, and $\log_x$ for elements with ACA > 1 ppm (rare instances of log scores >6 are cut to 6), and
4. scale to a fixed distance (10 units) from the origin.

The value of x in $\log_x$ is chosen such that a concentration of 100% returns a log score of 6. Average crustal abundance values are those of Rudnick and Gao (2003). For the data presented here, half the limit of detection is higher than ACA for Re (0.005 ppm) and Te (0.01 ppm).

Data below ACA are censored in Step 1 to reduce the effect of lithological signals. Given that ore-grade concentrations are typically at least two or three log units above ACA, variation in the data below ACA are very unlikely to be related to mineralisation and this variation is better removed. If the aim of the exercise is to model all of the variation in a dataset, all available elements should be included and no censoring should be applied. However, in the case of modelling ore-element signatures, only a select suite of elements is relevant and even for these elements some of the variation in the data relates to other factors such as host rock.

In log-transformed data, the effect of data variations below ACA are substantial for some elements. Fig. 1 shows that, for the data presented in this paper, Fe values are spread over a greater range of log units below ACA than above ACA; and there is also a substantial spread of data below ACA for Ni, Zn and Cu. For the data presented here, other elements that have significant variation below ACA include, La, U, Pb, Bi and Co (not shown).

The aim of the OSNACA transform is to create a metric in Step 3 where all 24 elements are similarly scaled between zero and six such that each step above zero represents a comparable enrichment above ACA. Thus, log scores of zero represent average crustal abundance or lower, scores of one-two are anomalous to weakly mineralised, three are about ore grade, four-five are high to bonanza grade and six are ultra-high grade (or 100% concentration for elements with ACA > 1 ppm). Table 1 lists the raw element values that correspond to OSNACA scores from zero to six. It is acknowledged that "ore-grade" varies with geography, metallurgy, economic conditions and many other factors, but the OSNACA scores provide a universal framework with which to compare mineralised samples.

A further aim of the OSNACA Transform in Step 4 is to scale the data to a fixed distance from the origin so that the Euclidean distance between any two points is a measure of geochemical similarity. Two samples with similar ore element signatures define enrichment vectors in similar directions away from the origin (ACA) and have a small distance between points. Conversely, two samples with different ore element signatures have enrichment vectors that are far apart and a commensurately large distance between points (Fig. 2). Ore-element signatures are not defined by overall abundance (grade), rather they are a function of ore-element ratios, hence Step 4 in the OSNACA transform to scale all data to the same distance from the origin.

Both the log-transform, and the Centred Log Ratio (CLR) transform (Aitchison, 1986) model all of the variation in a given data set. To the authors' knowledge, the OSNACA-transform is the only technique that attempts to isolate variation owing to mineralisation. The log-transform returns very different results for high-grade and low grade samples with the same ore element signature (same inter-element ratios). Conversely, CLR-transform is largely grade independent returning the same coordinates for samples which have identical inter-element ratios. The OSNACA-transform is similarly grade independent (Fig. 2), but is preferred here because inter-element ratios are only compared for elements enriched above ACA (i.e., those elements that are likely to be hosted by sulphide and oxide minerals). Comparisons between the CLR and OSNACA-transforms are discussed further below.

3. Data

The amount of publicly available geochemical data for ore deposits is extensive, but analytical techniques, detection limits, and above all, assay suites, vary widely. These inconsistencies limit the statistical procedures that can be applied to published data. For example, it is not practical to apply the OSNACA transform to published data because the subset of samples that have been analysed for all 24 ore and pathfinder elements used here, with appropriate detection limits, is extremely limited. In response to this gap in available data, researchers at the Centre for Exploration Targeting, University of Western Australia, Australia, created the OSNACA database, a publicly available on-line resource providing consistent high-quality geochemical data for metallic ore deposit samples from around the world (OSNACA, 2015).

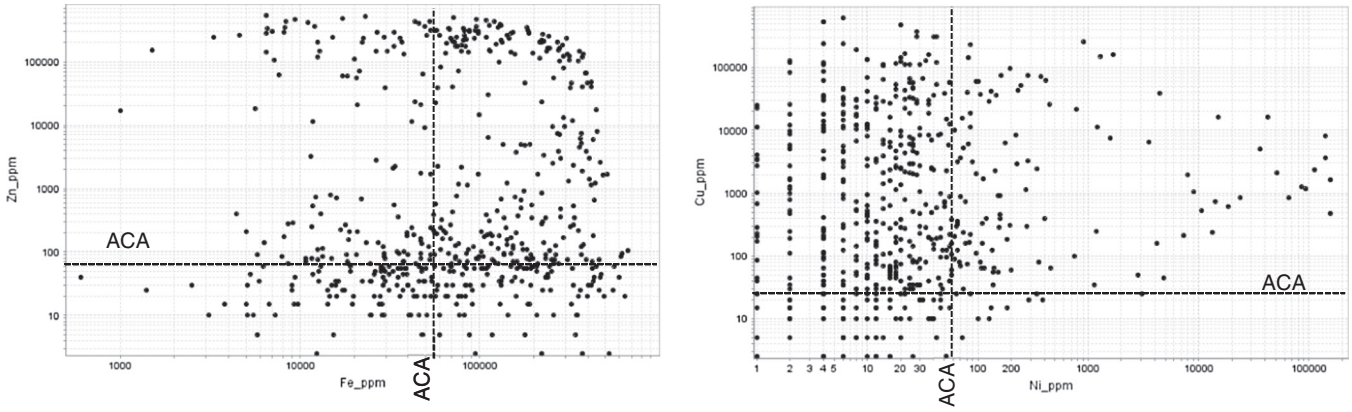

Fig. 1. Data distributions for OSNACA data relative to ACA for Fe-Zn and Ni-Cu.

Table 1
Raw element values corresponding to scores of 0–6 for each of the 24 elements in the OSNACA transform. Values in ppm unless otherwise stated.

Score	Fe	Co	Ni	Re	Pd	Pt	Cu	Ag	Au	Zn	Cd	In	Tl	Pb	Hg	As	Sb	Bi	Te	Mo	W	Sn	La	U
0	5.2%	27	59	0.19	0.0015	0.0015	27	0.056	0.0013	72	0.08	0.052	0.5	11	0.03	2.5	0.2	0.18	0.001	0.8	1	1.7	20	1.3
1	8.5%	160	300	1.9	0.015	0.015	160	0.56	0.013	350	0.8	0.52	5	74	0.3	21	2	1.8	0.01	8	10	16	120	12
2	14%	900	1520	19	0.15	0.15	900	5.6	0.13	1730	8	5.2	50	500	3	180	20	18	0.1	80	100	140	740	120
3	23%	5200	7700	190	1.5	1.5	5200	56	1.3	8500	80	52	500	3300	30	1580	200	180	1	800	1000	1300	4500	1140
4	37%	3.0%	3.9%	1900	15	15	3.0%	560	13	4.2%	800	520	5000	2.2%	300	1.4%	2000	1800	10	8000	1%	1.2%	2.7%	1.1%
5	61%	17%	20%	1.9%	150	150	17%	5600	130	20%	8000	5200	5%	15%	3000	12%	2.0%	1.8%	100	8%	10%	11%	16%	10%
6	100%	100%	100%	19%	1500	1500	100%	5.6%	1300	100%	8%	5.2%	50%	100%	3%	100%	20%	18%	1000	80%	100%	100%	100%	100%

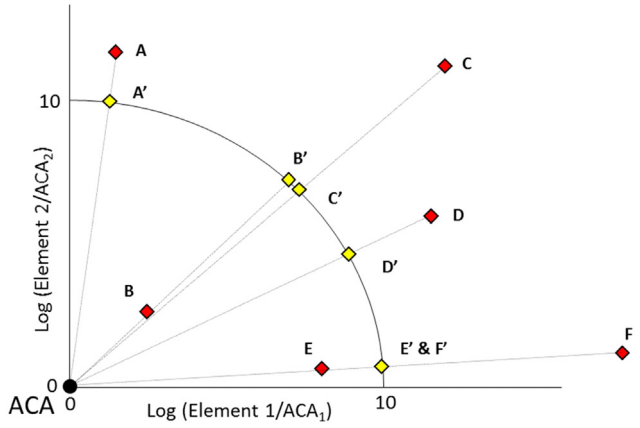

Fig. 2. Schematic depiction of the OSNACA transform for two elements. Data are censored to ACA, divided by ACA and then logged (red symbols). Data are then scaled such that each sample lies a fixed distance from the origin (yellow symbols). Samples with similar element ratios (similar ore signatures) lie close together (e.g. B' and C' or E' and F'). (For interpretation of the references to colour in this figure legend, the reader is referred to the web version of this article.)

Data presented here are for 573 samples from a current database of 683 samples, not including standards and duplicates, and come from mineral deposits from around the world (Fig. 3). Iron and pegmatite ore samples have been excluded because they are not well discriminated by the 24 elements that define MH-Space. Eighty one samples that are either weathered, or do not contain at least one commodity above the following ppm cut-offs, have also been excluded as not representing hypogene ore-grade material: Au(0.2), Pt(0.2), Pd(0.2), Ag(50), Cu(2000), Mo(250), Ni(2000), Pb(10000), Sn(2000), U(500), W(2000), Zn(10000).

Ore samples were analysed for 62 elements at Bureau Veritas Ultratrace Laboratories, Perth, Australia, by ICP-MS and ICP-OES following acid digests appropriate to each element. The four digests used were (1) Fire Assay, (2) Peroxide Fusion, (3) Aqua Regia, and (4) Mixed Acid (Hot Box). Further details on analytical technique are available on the OSNACA website (OSNACA, 2015).

Ore samples have been classified according to the notes provided by the sample donor (OSNACA, 2015). For presentation purposes, the ore deposit classification scheme used by OSNACA (2015) has been simplified into 16 classes as follows (number of samples in brackets):

1. Carlin Au (11)
2. Epithermal (72)
3. Orogenic-Au (147)
4. Porphyry Cu (29)
5. Porphyry Mo (5)
6. IOCG (30)
7. VHMS (80)
8. Sn-W (22)
9. Skarn-Manto (16)
10. Sediment-Hosted Cu (28)
11. SHMS (23)
12. Structural Pb-Zn (6)
13. Sandstone Pb-Zn (4)
14. MVT (51)
15. Magmatic Ni-Cu-PGE (22)
16. Other (27)

The orogenic-Au category includes Intrusion-Related-Au deposits and MVT includes Irish-type Pb-Zn deposits. Tin and W-skarns are not included in the skarn class, but grouped with Sn-W deposits instead.

Fig. 3. Global distribution of OSNACA samples at 1 December 2015.

4. Three dimensional reductions of MH-Space

4.1. Multidimensional scaling

Multi-Dimensional Scaling (MDS) is a statistical technique with similarities to principal component analysis (PCA) where the first multivariate component is defined to maximise variation, and then all subsequent components are defined to maximise the remaining variation. In PCA there are as many components as variables, whereas in MDS the number of dimensions is predetermined. MDS co-ordinates have been calculated in three dimensions for the global dataset of 573 samples. In addition to OSNACA-transformed data, MDS co-ordinates have been calculated for log and CLR-transformed data. This allows comparison of the three transforms before proceeding to further manipulations of the data (Fig. 4).

MDS plots for log-transformed and CLR transformed data are very similar but for OSNACA-transformed data MVT, SHMS and VHMS populations are more tightly defined, particularly on MDS1 vs MDS2 (Fig. 4). Overall, this leads to a clearer definition of the geochemical transition from MVT samples, through SHMS and VHMS samples to Cu-rich mineralisation. Magmatic Ni-Cu-PGE samples are discriminated on all three MDS1 versus MDS3 plots. Orogenic-Au samples extend from an area close to porphyry copper samples to an area occupied by Carlin-Au and some epithermal samples. This relationship is clearest on the MDS1 versus MDS2 plot for OSNACA-transformed data (Fig. 4c).

Analysis of Variance (ANOVA) has been calculated on MDS1–3 for both OSNACA and CLR transforms to test intra-class versus inter-class variance in the 15 simplified ore deposit classes. "Other" samples have been excluded because they do not represent a coherent population. The sum of F-scores for MDS1–3 is 267 for the OSNACA transform compared to 259 for the CLR transform, indicating similar overall between-group-variance/within-group-variance.

4.2. Principal component analysis

Principal Component Analysis of the 573 sample OSNACA-transformed data set provides results comparable to MDS. Discrimination of the various sample populations is not as clear for PC1 vs. PC2 as MDS1 vs. MDS2, but magmatic Ni-Cu-PGE and granitoid-hosted sample populations are better discriminated by PC3 than MDS3 (Figs. 4c and 5).

An ANOVA for PCs 1–8 calculated for OSNACA and CLR-transformed data shows that the OSNACA-transformed data more clearly discriminate the 15 ore deposit classes (Fig. 6). The sum of F-scores of 406 for the OSNACA transform is significantly higher than 274 for the CLR-transformed data, and most of the difference between the transforms is in PCs 1–3. Although an exhaustive statistical comparison has not been conducted between the OSNACA and CLR transformed data, visual inspection (Fig. 4) and ANOVA of PC1–8 (Fig. 6) suggest that the OSNACA transform better discriminates the 15 major ore deposit classes.

The plots of MDS1–3 and PC1–3 for OSNACA-transformed data suggest that MDS1-MDS2-PC3 may provide the best three dimensional reduction of 24-dimensional MH-Space. To test which three-dimensional framework most closely recasts 24-dimensional MH-Space, inter-sample distances in MDS1–2–3, PC1–2–3 and MDS1-MDS2-PC3 space are plotted against the corresponding distances in 24-dimensional MH-Space (Fig. 7). Three dimensional MDS space has a closer correlation to 24-dimensional MH-Space than three-dimensional PCA space but the closest correlation ($r^2 = 0.75$) is provided by MDS1-MDS2-PC3 space (Fig. 8). It is on this basis that MDS1-MDS2-PC3 axes are used here to present MH-Space in 3 dimensions.

4.3. Visualisation of MDS1-MDS2-PC3 space

Fifteen populations of ore deposit class besides "Other" have been wire-framed using Leapfrog so that they can be visualised in three

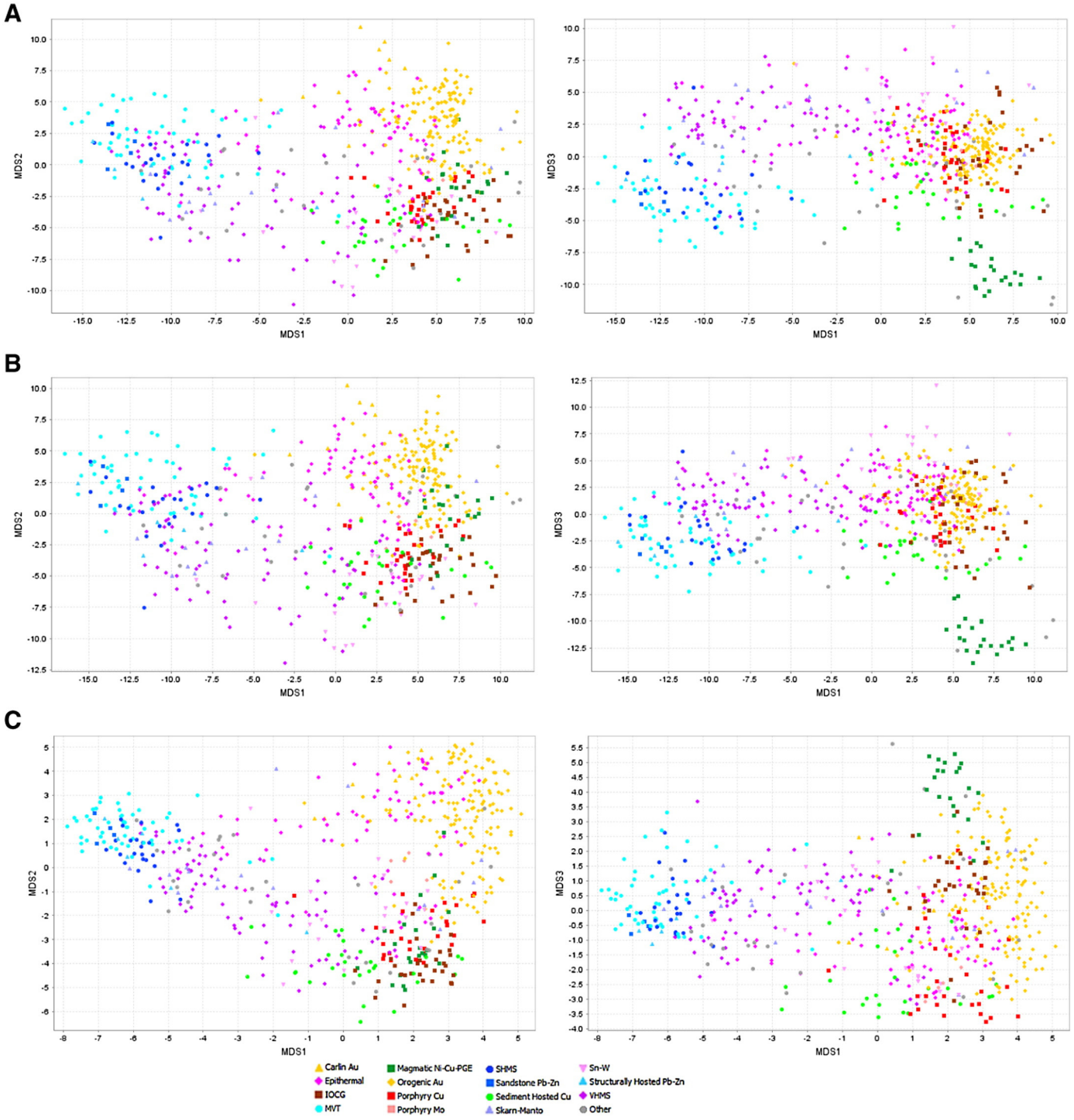

Fig. 4. MDS1 vs. MDS2 and MDS1 vs. MDS3 plots of 573 OSNACA samples for (A) log-transformed data, (B) log-centred transformed data and (C) OSNACA-transformed data.

dimensional MDS1-MDS2-PC3 space (Fig. 8). The relationships shown on Figs. 4 and 5 are readily apparent. Although a three dimensional representation of MH-Space sacrifices some accuracy, it represents one of the best ways to illustrate the overall architecture of MH-Space.

The transition from MVT samples, through SHMS and VHMS samples to samples of Cu-Au rich mineralisation is shown; so too the extension of orogenic-Au samples away from Cu-Au rich deposit classes to the Carlin-Au sample population. These are two of the major trends identified in MH-Space; Zn to Cu-Au and Cu-Au to Au only (Fig. 8a). The majority of epithermal samples define a population that connects these two trends by extending from Carlin-Au and orogenic-Au across to the VHMS and SHMS sample populations. This trend of epithermal samples corresponds to the low-sulphidation to high-sulphidation epithermal transition.

A third major trend in MH-Space from ultramafic to felsic extends from the magmatic Ni-Cu-PGE population through IOCG and orogenic-Au samples to porphyry Cu and more felsic rock associated examples of orogenic-Au and IOCG, to porphyry-Mo and Sn-W deposits

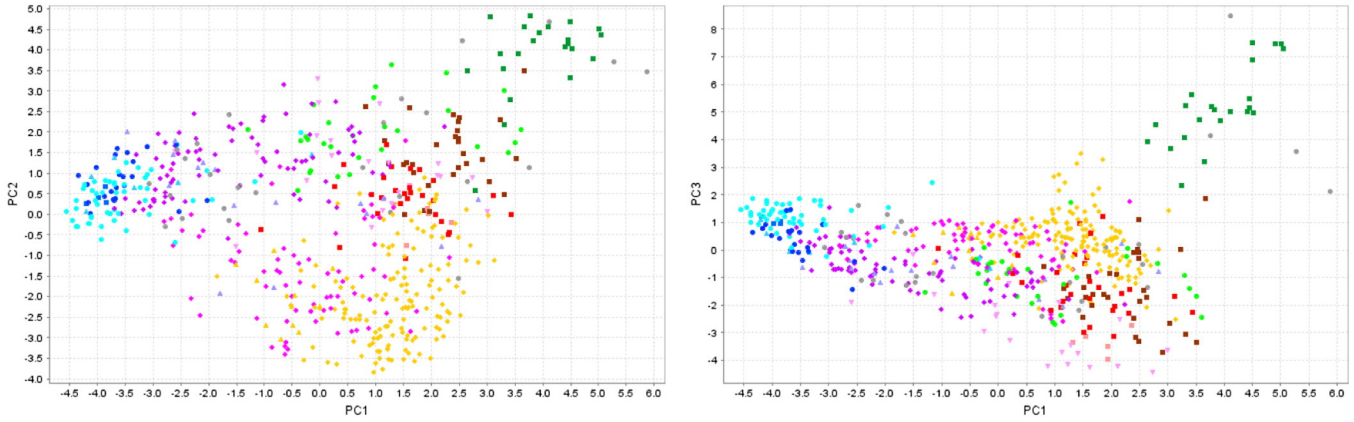

Fig. 5. PC1 versus PC2 and PC3 for 573 OSNACA-transformed data. Legend as for Fig. 4.

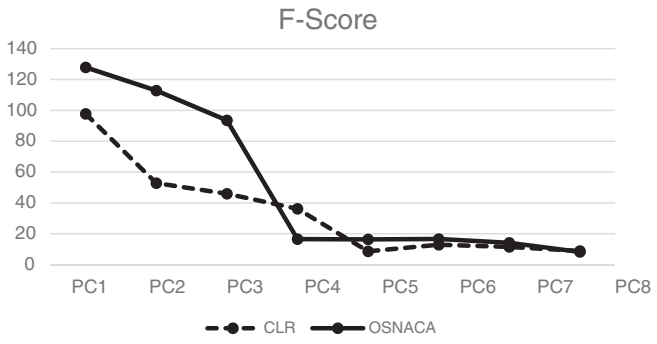

Fig. 6. F-scores from ANOVA in PC1–8 for OSNACA and CLR transformed data.

(Fig. 8b). Most samples in the view shown in Fig. 8b lie along the main "hydrothermal plane", with ultramafic associated mineralisation below and granitoid associated mineralisation above. The main "hydrothermal plane" contains the Zn to Cu-Au and Cu-Au to Au only trends shown in Fig. 8a but in Fig. 8b the transition from sediment-associated to igneous-associated deposit classes is more obvious. Magmatic Ni-Cu-PGE samples are clearly separated from other classes but some IOCG samples (particularly one each from Sossego, Brazil and Mount Elliot in Queensland) define a "keel" that extends down in the magmatic Ni-Cu-PGE direction. Samples of skarn mineralisation (largely obscured in Fig. 8) and Sn-W mineralisation are more widely scattered than other sample populations. This is not surprising for skarn samples which include samples from Zn-skarn, Au-skarn and manto deposits.

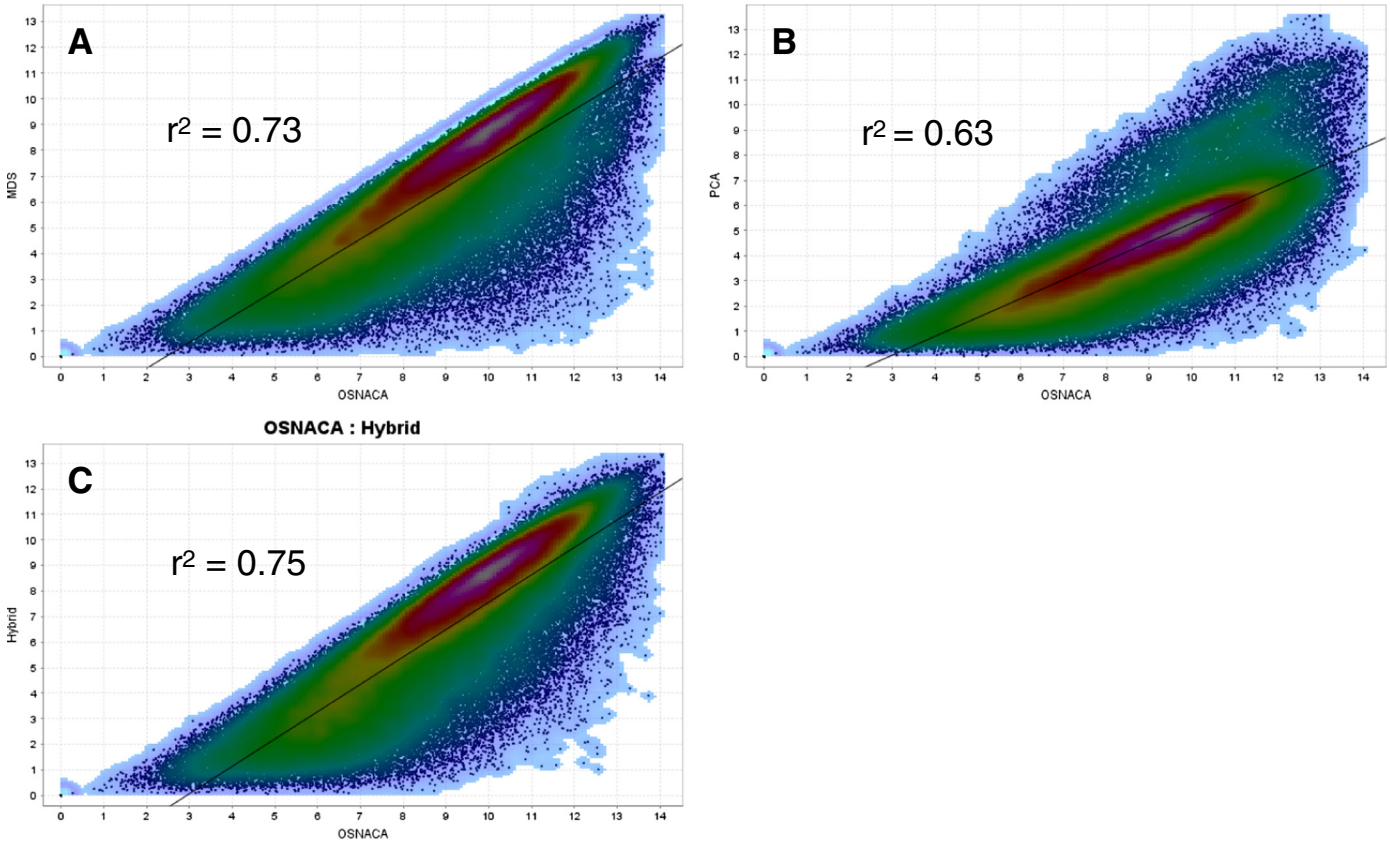

Fig. 7. Inter-sample distances in 24-dimensional OSNACA space versus (A) MDS1-MDS2-MDS3 space, (B) PC1-PC2-PC3 space, and (C) MDS1-MDS2-PC3 space.

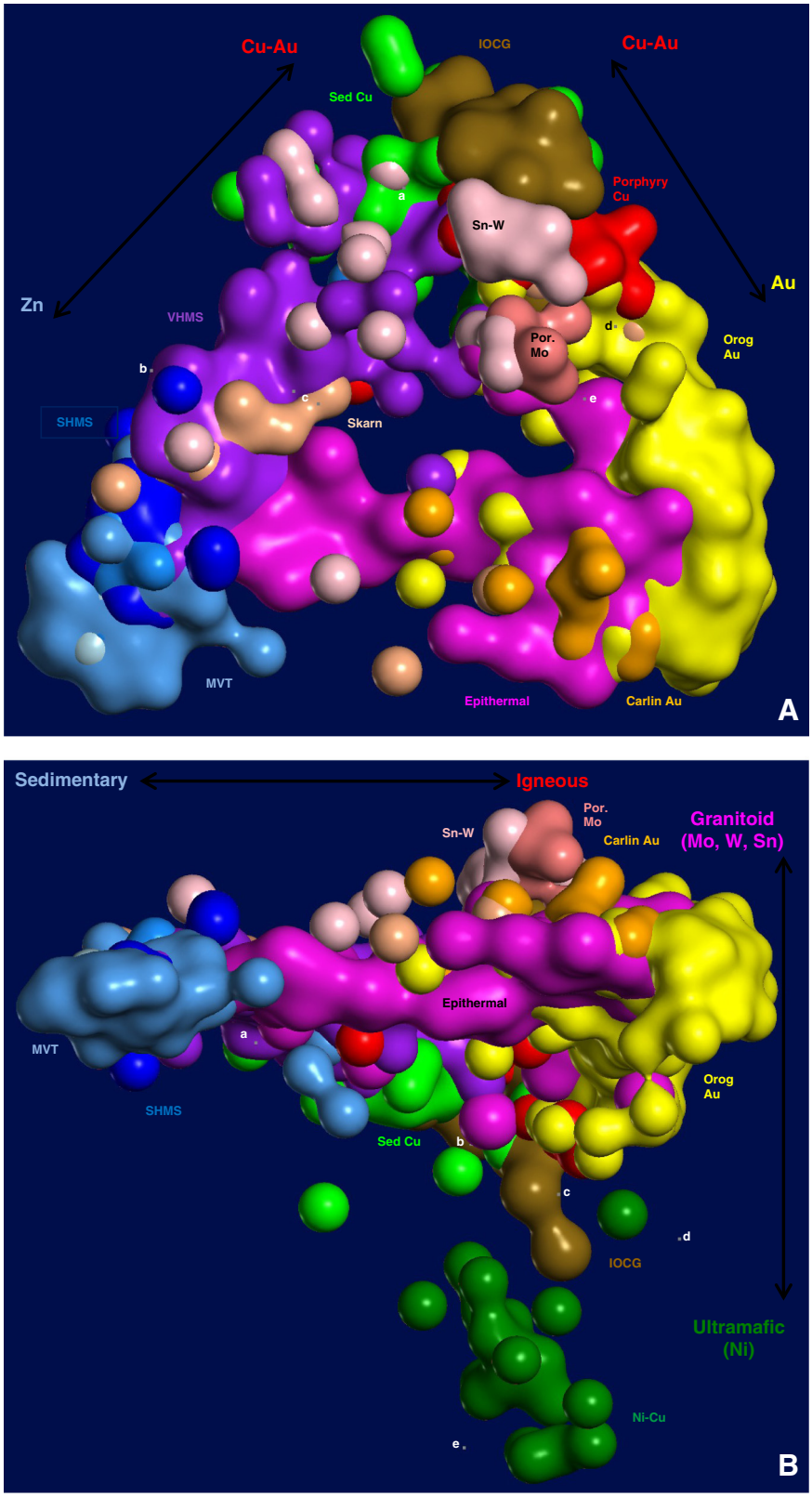

Fig. 8. Three dimensional views of MDS1-MDS2-PC3 space for 573 OSNACA-transformed ore deposit samples. (A) Zn to Cu-Au axis in MH-Space defined by transition from MVT through SHMS and VHMS to copper-rich classes. Cu-Au to Au axis defined by transition from copper rich classes to orogenic Au and Carlin Au. View is from –PC3, with Sn-W and porphyry Mo in the foreground and obscuring the magmatic Ni-Cu-PGE polygon in the background. "Other" samples that are not wire-framed are (a) Abra, (b) Broken Hill, (c). Abra (2 samples), (d) Witwatersrand and (e) Witwatersrand. (B) Ultramafic to Granitoid axis defined by transition from magmatic Ni-Cu-PGE through IOCG through the main "hydrothermal plane" to granitoid associated Mo and Sn-W samples. Along the main "hydrothermal plane" there is a transition from largely sedimentary to largely igneous associated deposits. "Other" samples that are not wire-framed are (a) Magellan (Pb), (b) Phalaborwa (Cu-Au-REE), (c) Enterprise (hydrothermal Ni), (d) Hunt (Au-Ni), and (e). Impala (Cr-PGE).

	Carlin	Epith	Oro-Au	Por-Cu	IOCG	VHMS	Skarn	Sn-W	Sed-Cu	SHMS	MVT	Ni-Cu
Carlin	4.2	7.2	7.1	9.3	9.9	8.6	9.4	8.5	10.5	9.2	9.9	11.3
Epith	7.1	6.4	7.2	8.0	8.9	7.7	9.2	7.5	9.4	8.6	9.2	10.6
Oro-Au	7.1	7.2	6.5	8.3	8.8	9.2	9.6	8.6	10.2	10.8	11.3	10.4
Por-Cu	9.3	8.0	8.3	5.8	6.9	8.1	8.5	8.3	7.2	10.4	11.2	9.8
IOCG	9.9	8.9	8.8	6.9	5.5	8.0	8.6	8.6	7.8	10.7	11.6	9.0
VHMS	8.6	7.7	9.2	8.1	8.0	5.3	7.9	6.4	8.5	6.3	7.4	10.4
Skarn	9.4	9.2	9.6	8.5	8.6	7.9	6.5	8.3	9.3	9.3	10.6	11.1
Sn-W	8.5	7.5	8.6	8.3	8.6	6.4	8.3	6.4	9.3	7.3	8.1	10.6
Sed-Cu	10.5	9.4	10.2	7.2	7.8	8.5	9.3	9.3	6.4	10.3	11.2	10.2
SHMS	9.2	8.6	10.8	10.4	10.7	6.3	9.3	7.3	10.3	3.9	5.0	11.8
MVT	9.9	9.2	11.3	11.2	11.6	7.4	10.6	8.1	11.2	5.0	5.0	12.2
Ni-Cu	11.3	10.6	10.4	9.8	9.0	10.4	11.1	10.6	10.2	11.8	12.2	5.1

Fig. 9. Average inter-sample Euclidean distances between members of main ore deposit classes with >10 samples.

An interactive three-dimensional models of the same 573 sample dataset shown in Fig. 8 is available for download at OSNACA (2015).

4.4. 24-dimensional check of MDS1-MDS2-PC3 relationships

The "keel" of IOCG samples extending towards magmatic Ni-Cu-PGE samples (Fig. 8b) is not an artefact of reducing three-dimensional MH-Space from 24 dimensions. In 24 dimensional MH-Space, five of the ten closest samples to the magmatic Ni-Cu-PGE population (based on average Euclidean distance to each member of the magmatic Ni-Cu-PGE population) are IOCG samples including two from Sossego, in the closest four. Four of the other top ten samples are Ni-related from the "Other" population (2 Hydrothermal Ni, 1 Cr-Ni-PGE, and an orogenic-Au – magmatic-Ni-Cu-PGE hybrid sample). Thus, it is clear that out of the 15 major ore deposit classes, the IOCG population contains samples with the closest geochemical relationship to magmatic Ni-Cu-PGE mineralisation.

Inter-class relationships are tested further where the average Euclidean distance between all members of each major ore deposit class and all members of every other major ore deposit class have been calculated (Fig. 9). Populations with fewer than 10 samples

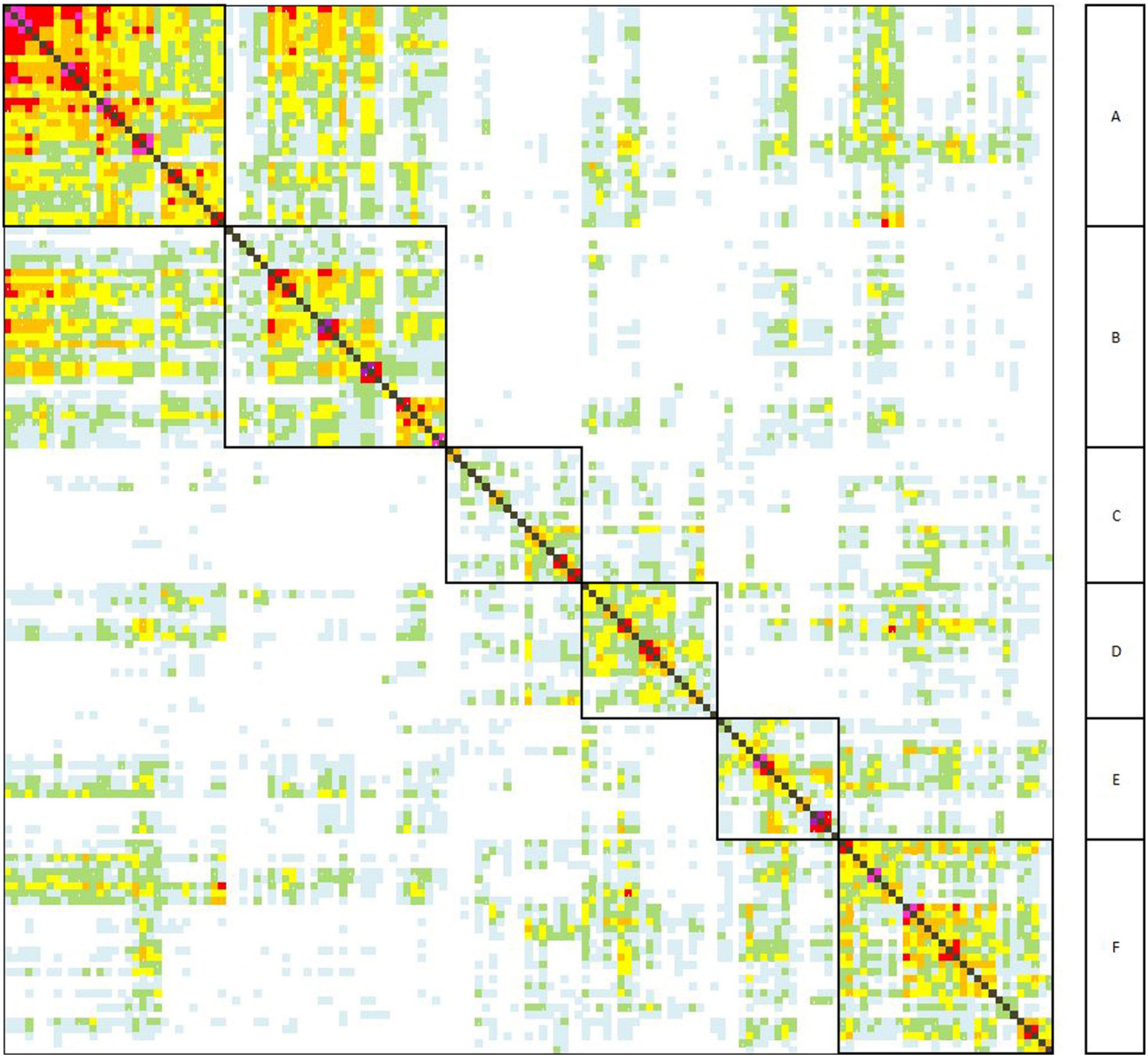

Fig. 10. Euclidean Distance Matrix for 147 orogenic-Au samples. Sample order determined by Ward clustering routine. "Hottest" colours represent most proximal sample pairs with smallest Euclidean distance. Sub-groups A–F outlined in bold. (For interpretation of the references to colour in this figure legend, the reader is referred to the web version of this article.)

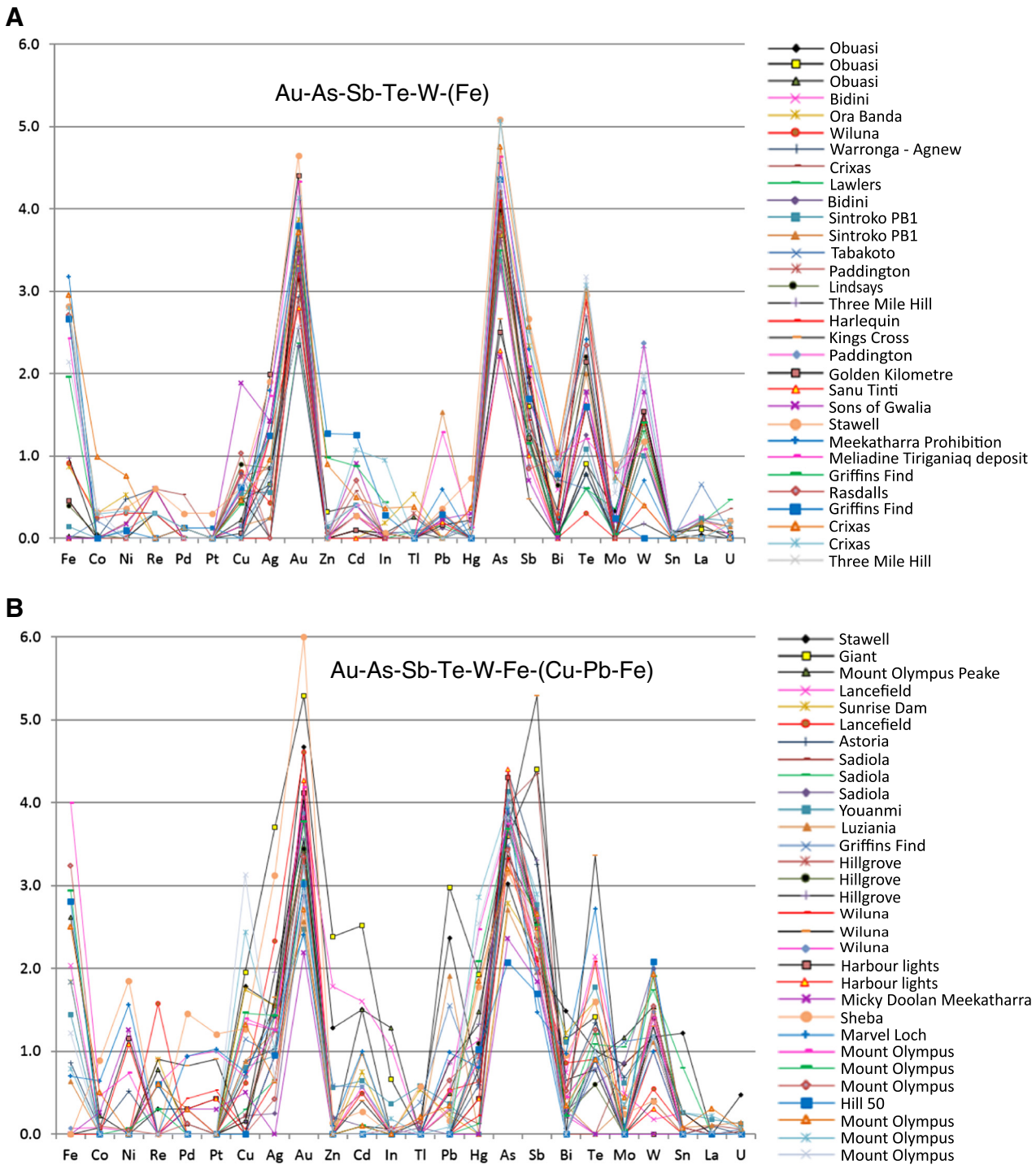

Fig. 11. Enrichment-plots for sub-groups A–F shown on Fig. 10.

have been excluded. The magmatic-Ni-Cu-PGE class has large average distances to every other class but its closest relationship is with the IOCG class. Other average distance relationships are consistent with the inter-class relationships shown in Fig. 8. Orogenic-Au, epithermal and Carlin Au classes are closest to each other, IOCG, porphyry Cu and sediment hosted Cu classes are closest to each other, and the SHMS and MVT populations are closest to each other just as they are on Fig. 8. The VHMS class is closest on average to the SHMS, Sn-W, MVT and epithermal classes (Fig. 9).

The average distance between sample pairs within each class gives an indication of the geochemical variation within each of the ore deposit classes.

In these data, SHMS and MVT sample populations have the lowest average inter-sample distances, corresponding to tightly constrained populations in three-dimensional MH-Space (Fig. 8). The most diverse metal signatures within a deposit class (average inter-sample distances >6.0) are found in the skarn, orogenic Au, Sn-W and epithermal classes. The wide scatter of skarn and Sn-W populations has been discussed

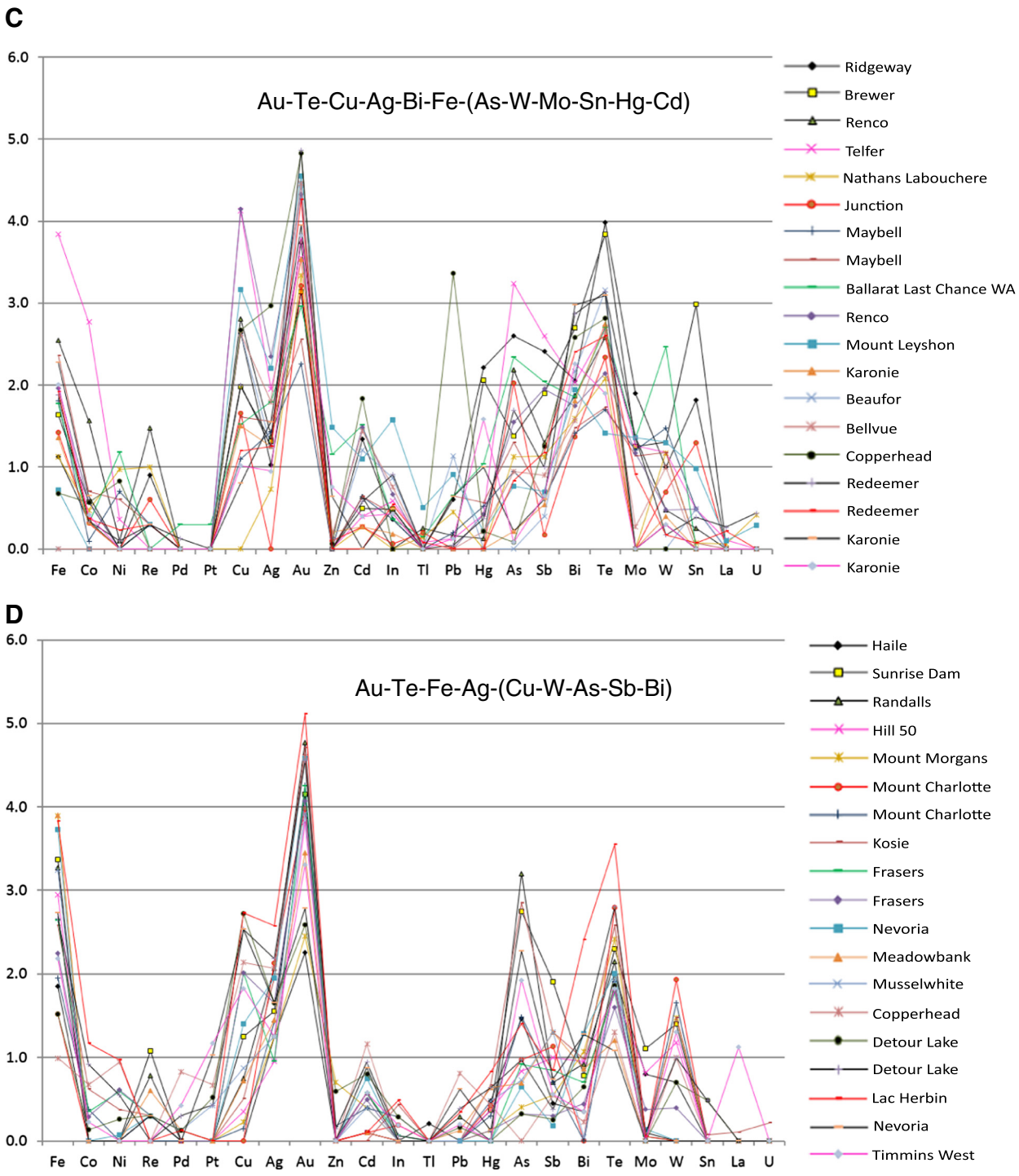

Fig. 11 (*continued*).

above. The large average inter-sample distance in the orogenic-Au and epithermal classes corresponds to the wide spread of samples in three-dimensional MH-Space. Orogenic-Au samples extend from the Carlin Au to porphyry Cu population and have a wide range of PC3 values. Epithermal samples are spread from SHMS-like signatures, to orogenic Au to porphyry Cu (Fig. 8).

5. Variations within deposit classes

Cluster analysis, following the methods of Fernández and Gómez (2008) has been employed to define sub-groups within four of the major ore deposit classes described above; orogenic-Au, VHMS, epithermal and sediment-hosted Cu. The Average, Weighted Average and Ward clustering routines were run for each class and the output that classified the samples into the most coherent sub-groups was chosen in each case.

Inter-sample distances from OSNACA transformed data can be used as the input for cluster analysis leading to sensible divisions very similar to those presented below. However, an orthonormal number space is preferred for this procedure, so scaled PCA scores calculated from OSNACA-transformed data are used as the input data. Principal Component Analysis yields an orthogonal dataspace and scaling the 24

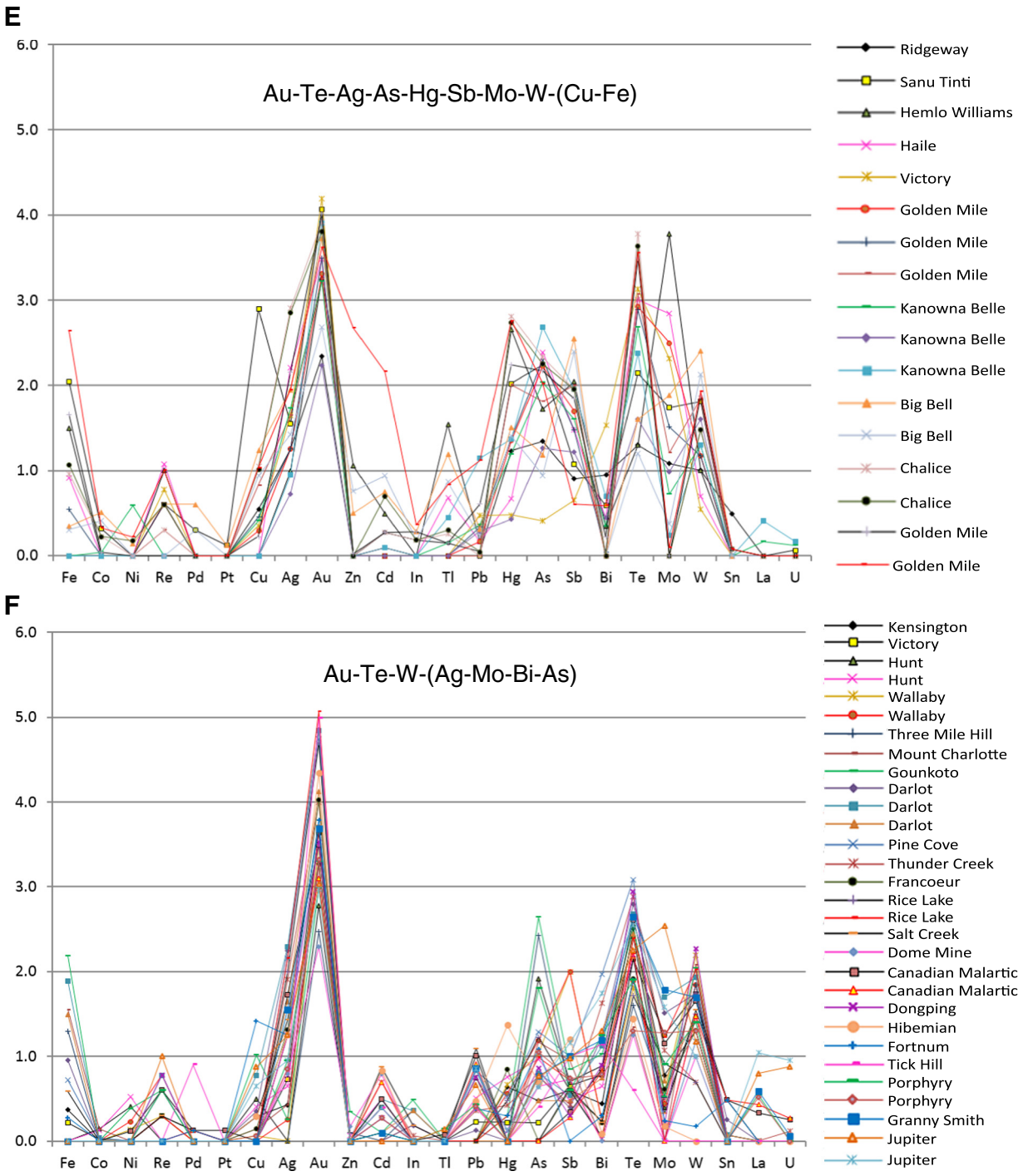

Fig. 11 (*continued*).

principal component scores so that each sample is the same distance from the origin yields and orthonormal space.

The Euclidean distance matrices below show the distance in 24 dimensional MH-Space between each sample and every other sample. They also list samples in the same order as the output from cluster analysis. By so doing, sub-groups identified by cluster analysis are immediately apparent and the effectiveness of the classification can be judged. Enrichment-plots presented below show unscaled OSNACA scores (Step 3 above) and are a graphical representation of the ore-element signature that defines each sub-group.

5.1. Orogenic-Au samples

The Ward clustering routine was selected as the best method for classifying 147 orogenic Au samples into sub-groups of like geochemical signature. Six sub-groups have been defined (Fig. 10). The starting sample for cluster analysis (an As-Sb rich sample from the Obuassi deposit in Ghana) was selected from one end of the orogenic-Au population (Fig. 8) away from other sample populations. The six sub-groups on Fig. 10 correspond to the six sub-groups represented on enrichment-plots (Fig. 11).

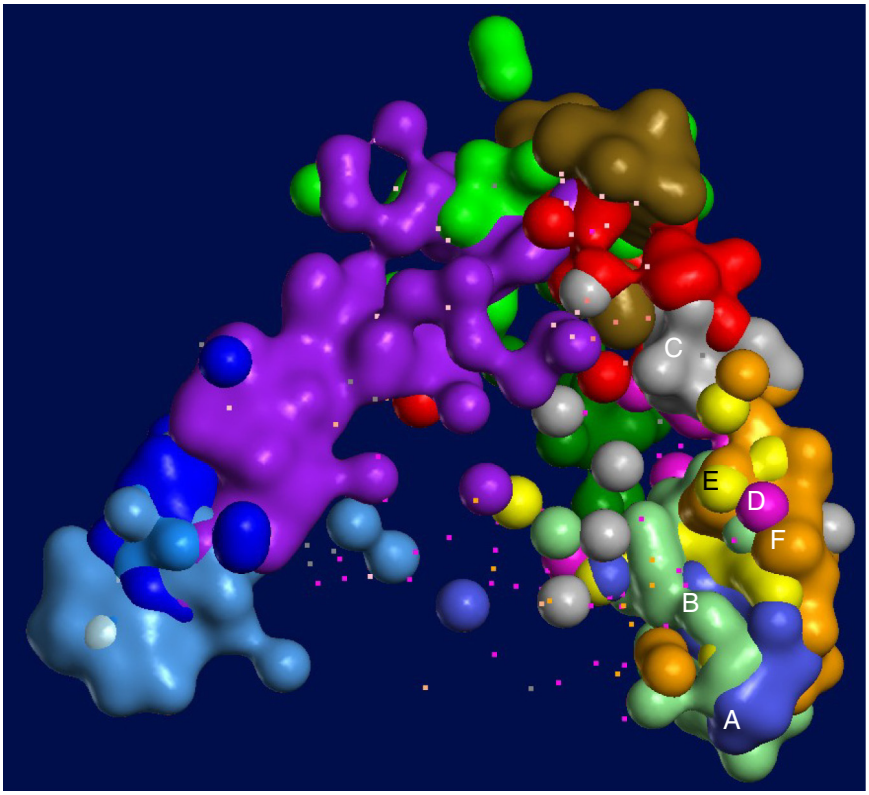

Fig. 12. View of orogenic-Au sub-groups A–F in MDS1-MDS2-PC3 space. Wire-frames for epithermal and Carlin Au samples removed for clarity.

Groups A and B are more closely related to each other than any of the other four sub-groups (Fig. 10) and they are the two sub-groups of orogenic-Au mineralisation strongly enriched in As-Sb (Fig. 11). Sub-group B has higher Fe, Cu, Pb and Te in most of its samples compared to sub-group A.

Most orogenic-Au samples are enriched in W but samples from sub-groups C and D are not as consistently enriched as the other four sub-groups. Sub-group C is the least well defined of the six sub-groups (Fig. 10) and has a correspondingly disordered enrichment-plot (Fig. 11c). However, sub-group C is marked by the highest Cu, Bi and Ag values of the six orogenic-Au sub-groups and has relatively high Fe for many its samples. Sub-group D, which has the most similarities to sub-group C on Fig. 10, has elevated Cu-Ag but not to the same degree as for sub-group C. It is also marked by distinctly higher Fe.

Sub-groups E and F have similar Au-Te-W enriched signatures with elevated Mo for many samples. Sub-group E samples are also distinctly elevated in Ag and Hg and have higher As and Sb than other samples in sub-groups C–F.

Wire-frame models of the six orogenic-Au sub-groups (Fig. 12) show that sub-groups C and D lie close to the Cu-Au rich ore deposit classes and sub-group C in particular overlaps with the porphyry-Cu class. This is in keeping with variable enrichments in Cu, Ag, Bi and Mo for samples in these two classes. Sub-group F has a more "felsic" signature with enriched Ag-Bi-Mo in many of its samples and lies in the foreground of Fig. 12 alongside granitoid-hosted mineralisation classes like Sn-W. Sub-group E is entangled with, but lies largely behind sub-group F (Fig. 12) and has a metal signature in between that of sub-groups A and C with moderately enriched As-Sb but also enriched in Ag $\pm$ Hg $\pm$ Mo.

Forty-one orogenic-Au deposits are represented by more than one sample in these data. Of these, samples for 28 deposits fall exclusively into one of the six sub-groups A–F. Of the 13 deposits with samples that fall into two sub-groups, five have sample pairs that fall in related sub-groups: A–B, C–D or E–F (Fig. 10). The remaining eight deposits are represented by sample pairs that lie in "unrelated" sub-groups but six of these "discordant" sample pairs are separated by Euclidean distances below 9.5 (green and yellow shading on Fig. 10).

These results suggest that in most cases a low number of samples can be used to quite tightly constrain the metal signature of an orogenic-Au deposit. It also shows that, although the sub-groups are useful to illustrate variations in orogenic-Au deposit geochemistry, the divisions are far from perfect. There is substantial overlap between sub-groups, such that every samples is closer to several samples from outside its sub-group than to the most distant sample within its own sub-group.

Host rock is not a dominant control on metal signatures in orogenic-Au deposits based on these data. Mafic and sedimentary rocks are the host to samples from all six sub-groups, although sedimentary host rocks feature more prominently in sub-groups A, B and D. The most distinct sub-group in terms of host rock is sub-group F where about half of the samples are granitoid hosted, accounting for most of the granitoid-hosted orogenic-Au samples in the database.

5.2. VHMS samples

A sample from the DeGrussa deposit in Western Australia lies at the "Cu-Au" end of the VHMS sample population in MDS1-MDS2-PC3 space (Fig. 8) and was used as the starting sample for cluster analysis. The Ward method of clustering was selected for sub-group classification (Figs. 13 & 14).

Sub-groups A and B are both populations of Cu-rich VHMS mineralisation, but sub-group A is distinguished by lower values for a number of elements, particularly Zn, Cd and Sn, but higher

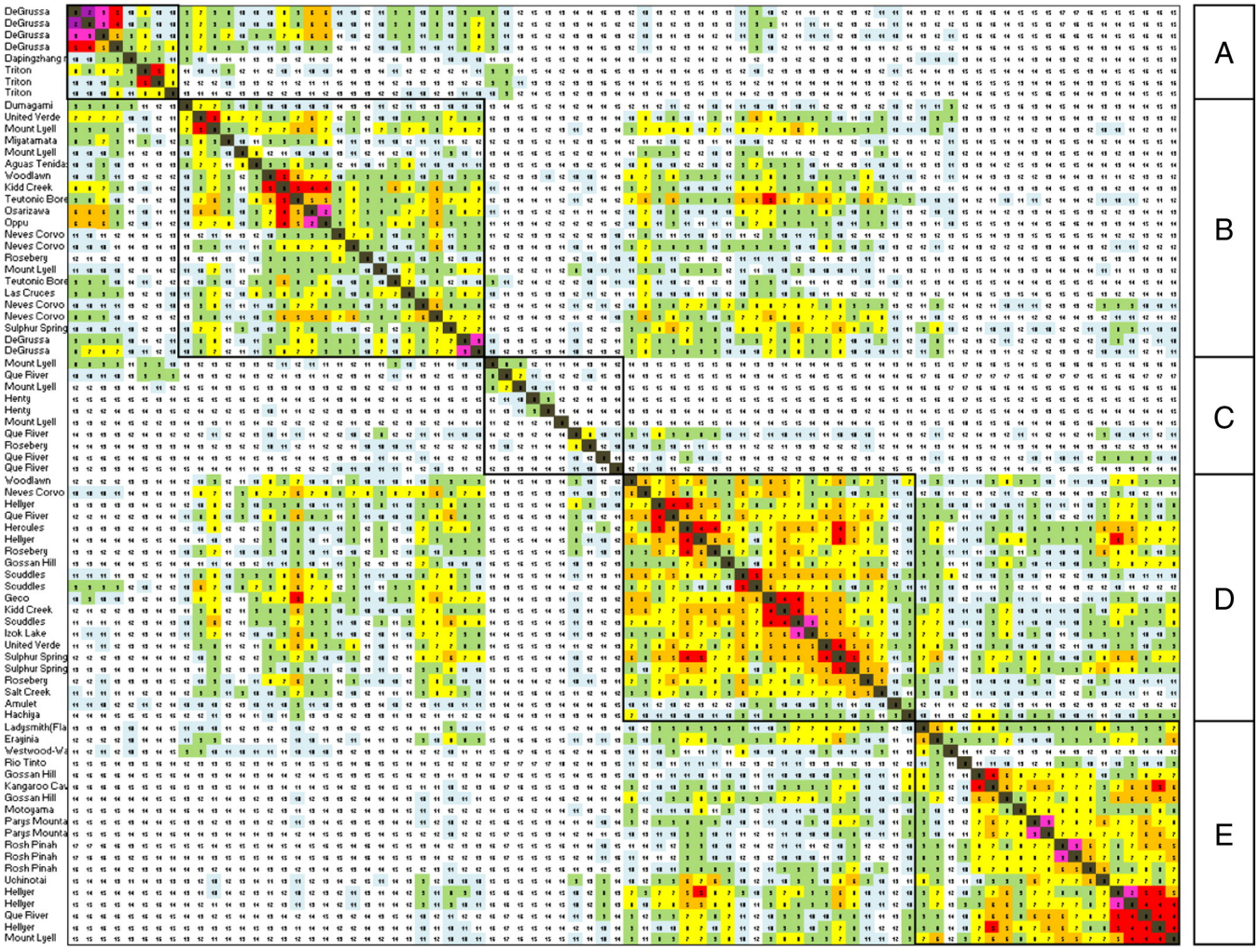

Fig. 13. Euclidean Distance Matrix for 80 VHMS samples, with samples ordered according to the Ward clustering method. "Hottest" colours represent most proximal sample pairs with smallest Euclidean distance. (For interpretation of the references to colour in this figure legend, the reader is referred to the web version of this article.)

Te (Fig. 14). Sub-group C samples have the lowest Zn-values and are characterised by a Cu-Au-Ag-As-Sb signature. Sub-groups D and E contain samples of Zn-rich VHMS mineralisation and have similar signatures reflected by their close relationship on Fig. 13. Sub-group D has higher In and Sn, but generally lower Te than sub-group E.

In three-dimensional MH-Space, the distribution of Cu, Cu-Zn and Zn-Cu enriched VHMS samples (Groups A, B and D–E respectively) follows the expected transition from Cu-Au enriched ore deposit classes to sediment-hosted Pb-Zn classes. Sub-group A intersects part of the porphyry Cu population, forming a discrete population adjacent to sub-group B, which in turn lies alongside sub-group D and then sub-group E which intersects the SHMS and MVT populations (Fig. 15). The wide scattering of samples in sub-group C (Figs. 13 & 14) is repeated in three-dimensional MH-Space, but these samples tend towards Cu-Au rich ore deposit classes (Fig. 15).

A number of deposits feature in more than one VHMS sub-class. Notably, there are Cu-Zn and Zn-Cu samples from the copper and zinc-rich portions of the Woodlawn, Kidd Creek, Rosebery, Mount Lyell, United Verde and Sulphur Springs deposits. Clearly this relates to the well documented zonation from Cu to Zn-rich VHMS ores (e.g., Lydon, 1984).

5.3. Epithermal samples

Seventy two epithermal samples have been classified into five sub-groups using the Average clustering method (Figs. 16 &17). The starting sample is a Zn-rich sample from the Equity deposit in Colorado which lies closest to SHMS samples in 3 dimensional MH-Space.

Group A is discriminated from the other four sub-groups by markedly higher Zn-Cd-Pb values (Fig. 17). Sub-group B comprises 22 samples including 17 from the Lake Cowal deposit in NSW which is the only ore deposit where detailed sampling has been undertaken thus far by the OSNACA Project (see below). It is marked by much lower, but still anomalous, Cu-Zn-Cd-Pb values compared to sub-group A, whereas sub-group C samples have virtually no base-metal enrichment and a simpler Au-Sb-Ag-As ± Te ± Hg ± Tl ± W signature. On a Euclidean distance matrix (Fig. 16) sub-group A is most similar to sub-group B, and sub-groups B and C also have a close relationship.

Group D has a signature closest to sub-group C, whereas sub-groups E contains samples of Au-Cu-Ag-Bi rich Epithermal mineralization. In 3 dimensional MH-Space sub-groups A–C span the gap between SHMS and Orogenic-Au samples, whereas sub-group E is located close to the porphyry Cu population (Fig. 18). Sub-group D samples are scattered around sub-groups B and C. These relationships between Zn-rich

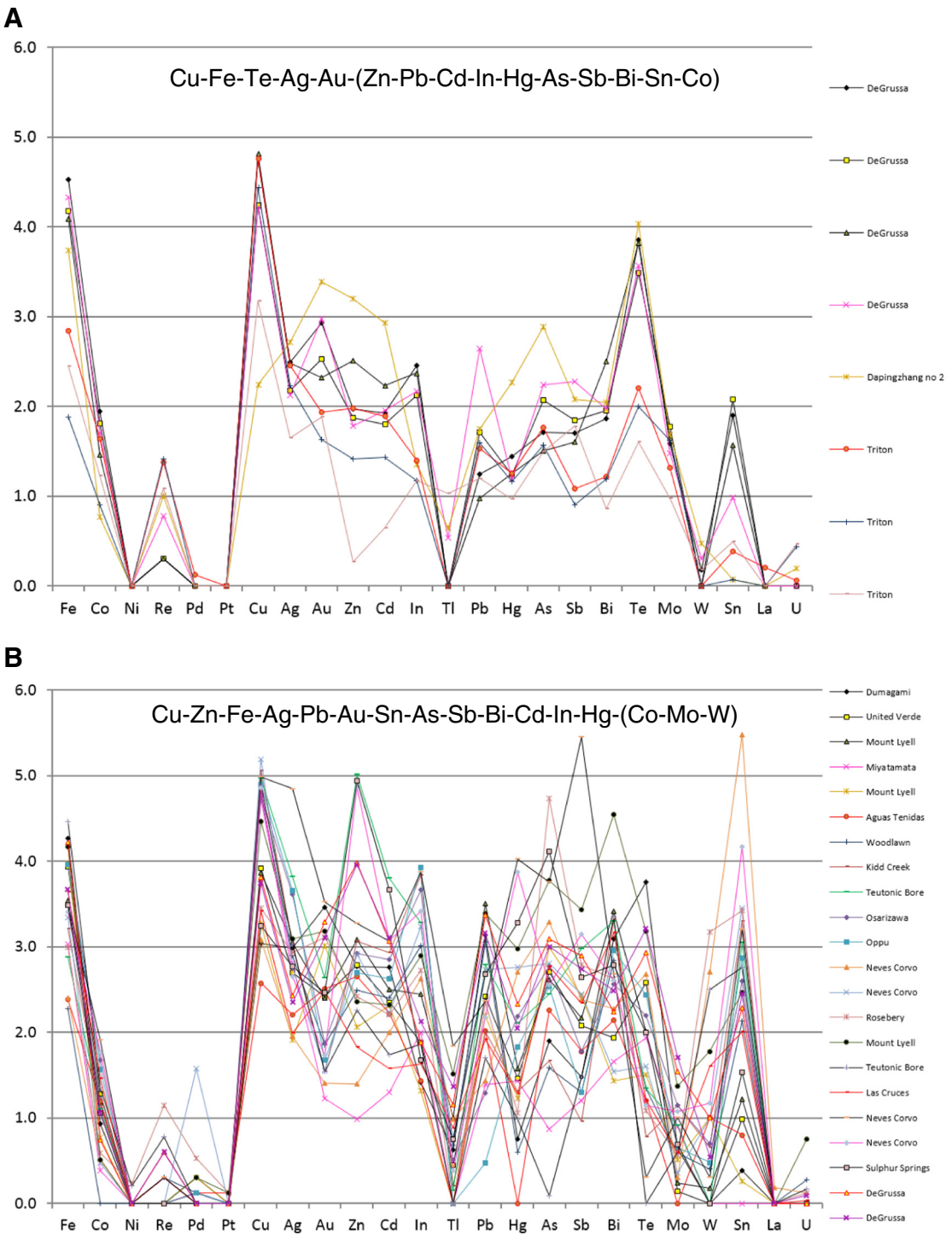

Fig. 14. Enrichment plots for VHMS sub-groups A–E shown on Fig. 13.

(Group A), base-metal poor (Group C) and Cu-rich (Group E) epithermal sub-groups are exactly what the global model of MH-Space (Fig. 8) predicts.

5.4. Sediment hosted copper samples

The OSNACA database contains only 28 samples of "ore grade" sediment hosted Cu mineralisation, but these samples have diverse metal enrichment signatures (Figs. 19 & 20). Using a sample from Mufulira in Zambia as the starting sample, the Ward clustering algorithm was used to classify six sub-groups. Sub-groups A–C have high Cu-Ag. Sub-group A also has high Bi-Au, whereas sub-group B of Polish samples from the Lubin and Rudna deposits has high Mo-Re, and sub-group C has elevated In-Sn-Au-Fe (Fig. 20). Sub-group D of African Copper Belt samples has a somewhat disparate metal signature. Sub-group E, also comprising African Copper Belt samples, has a Cu-Au-(Te-Mo-La-In-Re) signature, and sub-group F from Mount Oxide in Queensland has a Cu-Ag-As-Sb-Bi-Tl-Co signature.

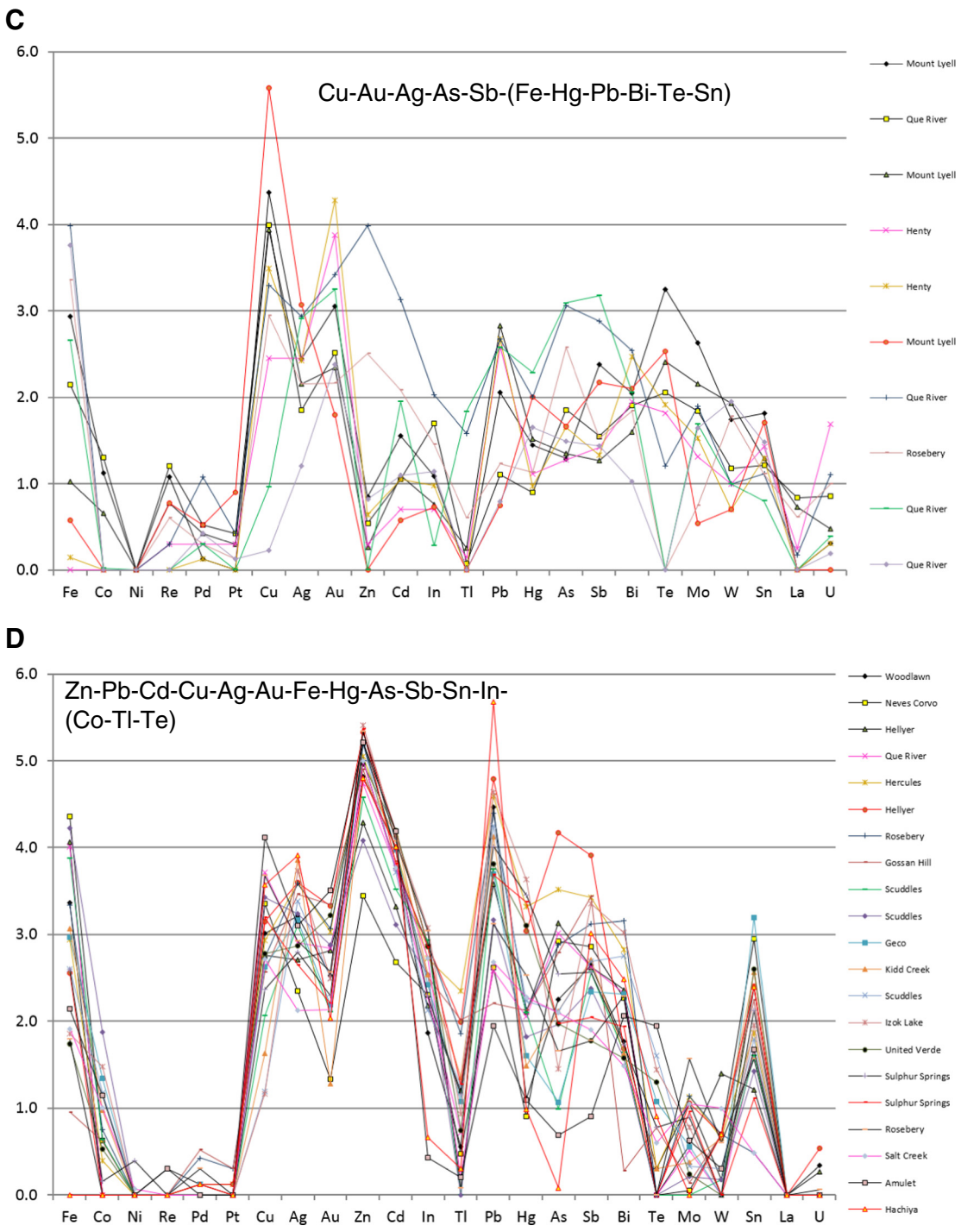

Fig. 14 (*continued*).

As expected, these diverse metal signatures lead to relationships in three-dimensional MH-Space that are not easy to interpret (Fig. 21). Perhaps of greatest significance is the separation of much of sub-group E (Cu-Au-(Te-Mo-La-In-Re) signature) from the other sediment hosted Cu subgroups. Much of the porphyry-Cu and IOCG populations (red and brown dots on Fig. 21) lie between sub-group E and the other sediment hosted Cu subgroups. The Cu-Au-(Te-Mo-La-In-Re) element association is difficult to reconcile with ore derived from a sedimentary basinal ore fluid, and is more suggestive of a magmatic affinity. Thus, deposits in sub-group E have been flagged for closer inspection and possible reclassification.

6. Intra-deposit variations: Lake Cowal

The Lake Cowal epithermal deposit in New South Wales is the only ore deposit in the OSNACA database where a sufficient number of accurately located samples have been collected to begin assessing intra-deposit variations in ore-element signatures. Nineteen out of 21 samples from Lake Cowal contain >0.2 g/t Au and these samples

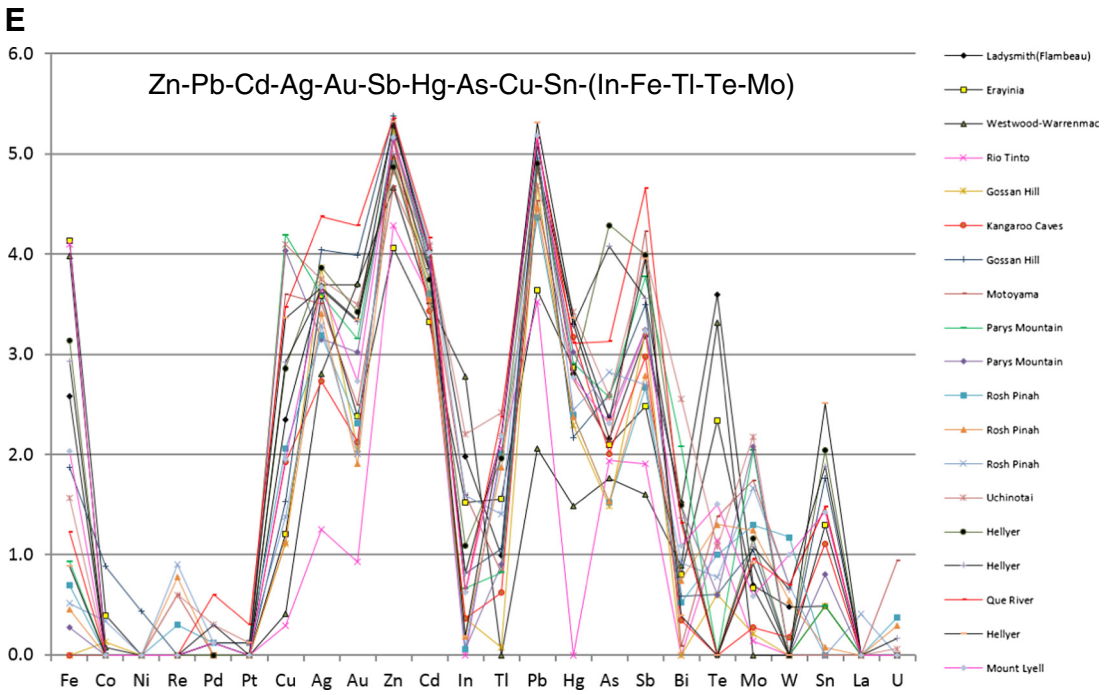

Fig. 14 (*continued*).

have been classified by the Average clustering routine to define four different sub-groups of metal signature (Figs. 22 & 23). The starting sample lies furthest from the other samples in MH-Space and it alone comprises sub-group A with the lowest overall metal content. There is a progressive increase in Zn-Cd-Pb-Hg-Te from sub-group A to sub-group D, with notably higher Cd-Zn in sub-group D which

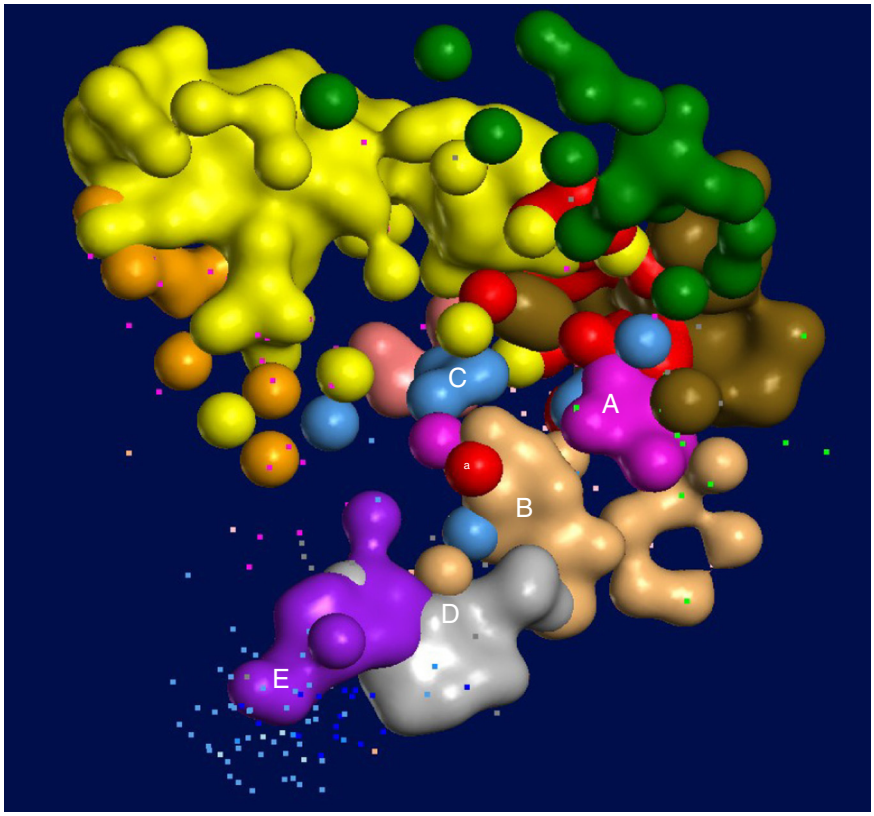

Fig. 15. View of VHMS sub-groups A-E in MDS1-MDS2-PC3 space. Wire-frames for MVT, sandstone Pb-Zn, structural Pb-Zn, SHMS, sediment hosted Cu, Sn-W and epithermal removed for clarity. Porphyry-Cu outlier (red) labelled a. is from the Los Bronces deposit in Chile. (For interpretation of the references to colour in this figure legend, the reader is referred to the web version of this article.)

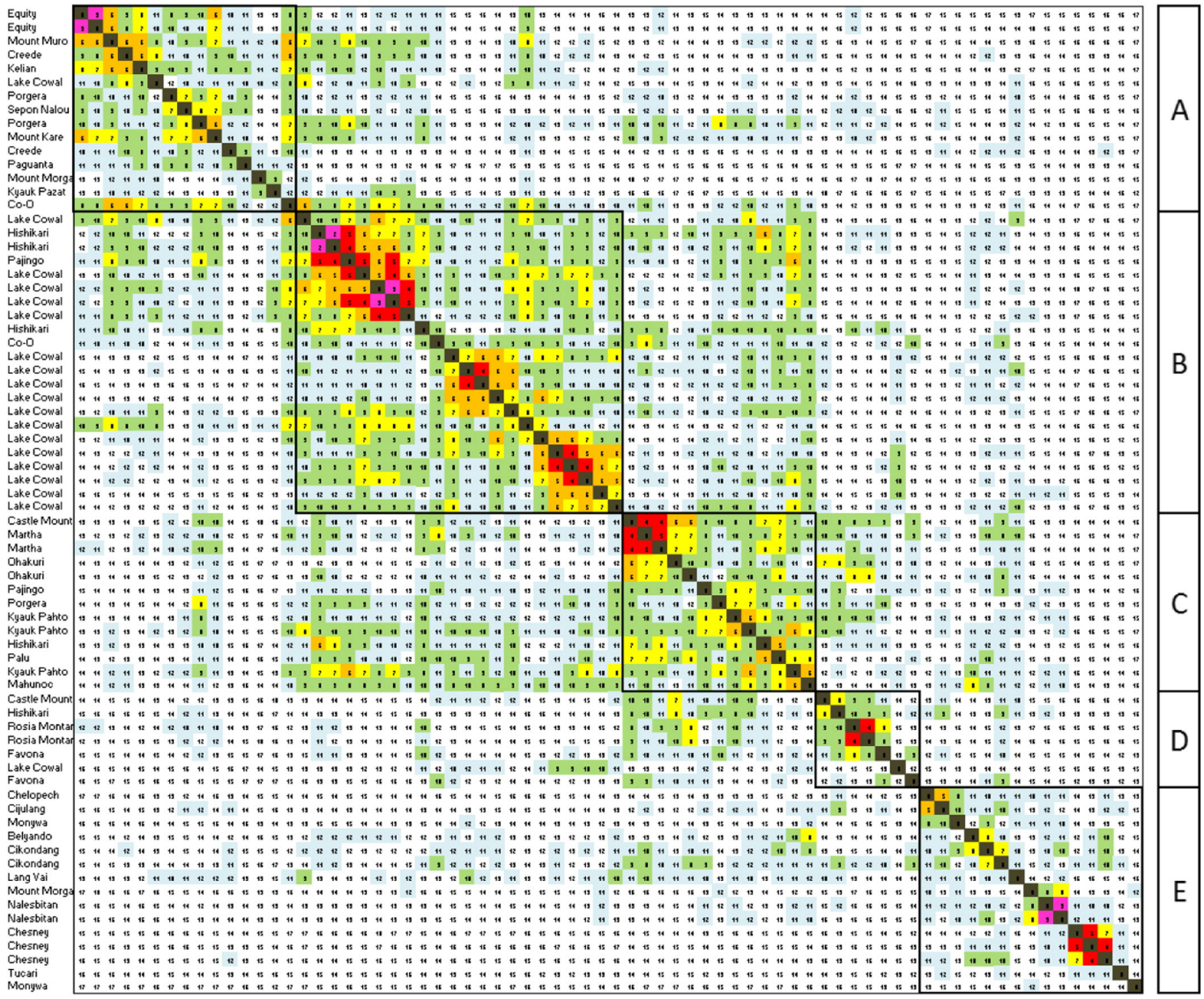

Fig. 16. Euclidean Distance Matrix for 72 epithermal samples. Sample order determined by Average clustering routine. "Hottest" colours represent most proximal sample pairs with smallest Euclidean distance. (For interpretation of the references to colour in this figure legend, the reader is referred to the web version of this article.)

also contains the richest Au samples (top three samples: 26–370 g/t Au).

In three-dimensional MH-Space the Lake Cowal samples take up much of the volume defined by epithermal sub-group B (Fig. 24). Lake Cowal sub-groups B-D trend from orogenic-Au space towards, but not nearly as far as, the Pb-Zn-rich deposit classes (Fig. 24). These results emphasise the point that individual ore deposits have a range of ore-element signatures. The 19 Lake Cowal samples define a coherent domain, but they occupy a volume rather than a point in MH-Space.

The spatial distribution of the four Lake Cowal sample sub-groups is indicative of metal zonation within the deposit. The sample comprising sub-group A lies in the south-west corner of the sampled area, sub-group B and C samples lie in the central and north-central parts of the open pit, and sub-group D samples dominate the western half of the sampled area (Fig. 25).

Naturally, a great deal more data is required to properly constrain metal zonation patterns at Lake Cowal or any other deposit, but these data do show that this approach to constraining metal signatures at the deposit-scale warrants further work. Most Lake Cowal samples place the deposit in epithermal sub-group B, suggesting that, although intra-deposit variations are significant, a handful of samples will adequately constrain such a deposit in global MH-Space.

7. Discussion

Numerous workers have suggested a geological continuum between different ore deposit classes such as MVT and SHMS (e.g., Leach et al., 2005), VHMS and epithermal (e.g., Hannington et al., 1999), porphyry-Cu and epithermal (Arribas et al., 1995), orogenic Au, Carlin Au and epithermal (Nesbitt, 1988) and even a link between IOCG deposits and mantle-related mineralisation such as carbonatites (Groves et al., 2010). The overlapping relationships between sample populations (Fig. 8) show that many of the transitions described by ore deposit researchers are mirrored in MH-Space. That is notwithstanding a very limited sample population for a global database, inevitable errors in deposit classification and limitations inherent in defining relationships between samples by geochemical means alone.

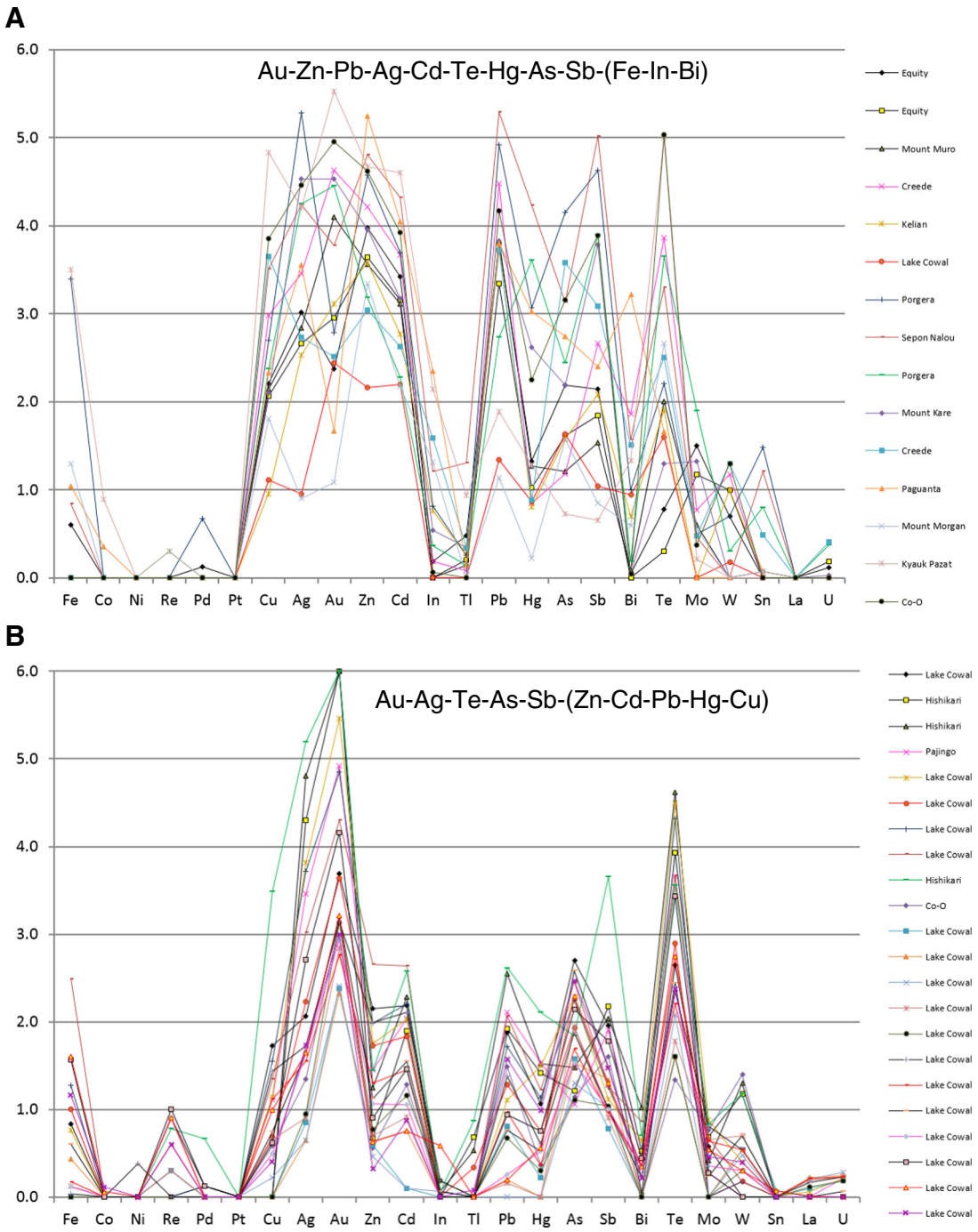

Fig. 17. Enrichment plots for epithermal sub-groups A–E shown on Fig. 16.

MH-Space provides a framework in which any metal enrichment found in nature can be mapped. The work presented here demonstrates that samples from individual ore deposit classes occupy discrete and predictable locations within that space. Individual mineral deposits occupy smaller volumes within the space defined by their class. Metal signatures that define individual ore deposits and ore deposit classes overlap to create the continuum shown in Fig. 8. The main trends of Zn to Cu-Au, Cu-Au to Au only and Ni to Sn-W define the gross architecture of MH-Space (Fig. 8) with more subtle variations in inter-element ratios defining intra-class and intra-deposit divisions.

7.1. Limitations

Paragenetic studies commonly show that an ore-grade sample is the product of multiple hydrothermal events. Therefore, each data point must be viewed as representing the combined effect of all metasomatic events that have affected that sample. Despite this limitation, it appears that the dominant mineralising event overwhelms other metal signatures in most cases. A sample of magmatic Ni-Cu-PGE mineralisation with an orogenic-Au overprint from the Hunt deposit in Western Australia (Fig. 8b) is the only clear example of mixed ore-element signatures in the database.

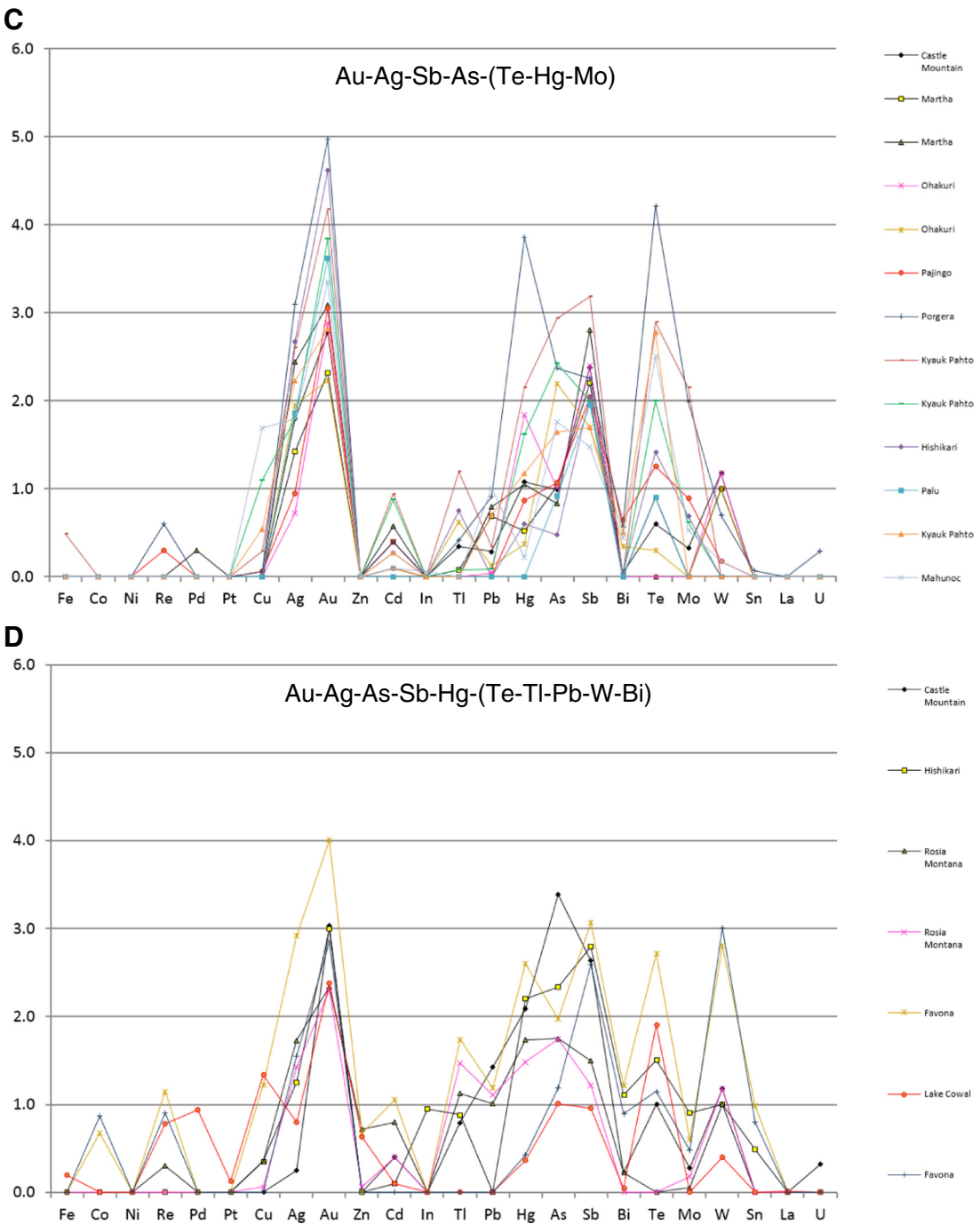

Fig. 17 (*continued*).

The OSNACA-transform attempts to remove variation in the data owing to lithology by removing values below ACA. However there are some lithological effects still evident in OSNACA-transformed data. Many of the "Fe-enriched" orogenic-Au samples are hosted by banded iron formation, so too a handful of Ni and Cu enrichments in orogenic-Au samples are a product of an ultramafic or mafic host rock. In orogenic-Au samples, Ni and Cu anomalies owing to lithology are all below OSNACA scores of two and generally below one so their effect is not as large as that for Fe (Fig. 11). In orogenic-Au and other deposit classes, the effect of high U, La and other incompatible elements in felsic host rocks also appears to be very minor with OSNACA scores greater than one attributable to host rock being very rare. Refining the cutoffs that remove variation in the data owing to lithology will complicate the OSNACA-transform but further work in this area is definitely warranted.

The OSNACA ore deposit classification system (OSNACA, 2015) attempts to be fairly broad, and readily accommodates most of the material donated. Whether a particular classification is "correct" is another matter. Disagreements over ore deposit classification are inevitable, so the most impartial approach is to classify each sample according to the donor's instructions. Where metal signatures suggest that some samples are misclassified (e.g., Fig. 20e), this inconsistency can be flagged.

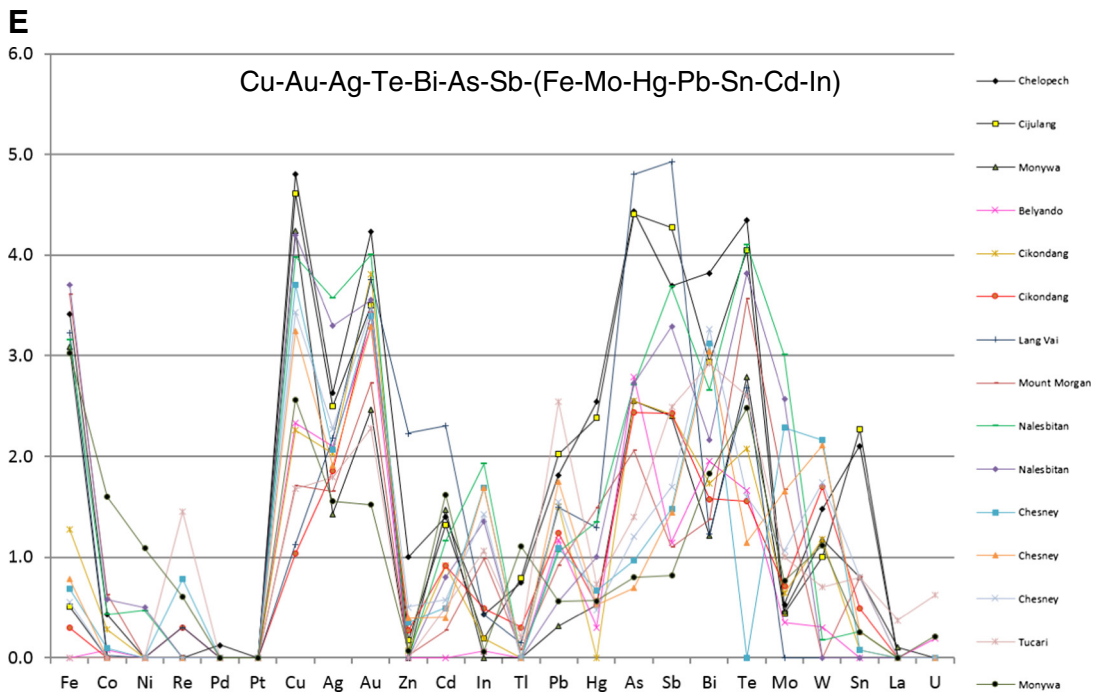

Fig. 17 (*continued*).

The three-dimensional simplification of MH-Space creates distortions, and this must be kept in mind when using this perspective. If the three-dimensional framework is used in conjunction with undistorted outputs from MH-Space like Euclidean distance matrices and enrichment-plots, the risk of misinterpreting the data is reduced. Limited data will always limit what conclusions can be drawn from the OSNACA database. Every ore deposit class will benefit from additional samples, but as it stands, porphyry-Cu is the most underrepresented major deposit class in the

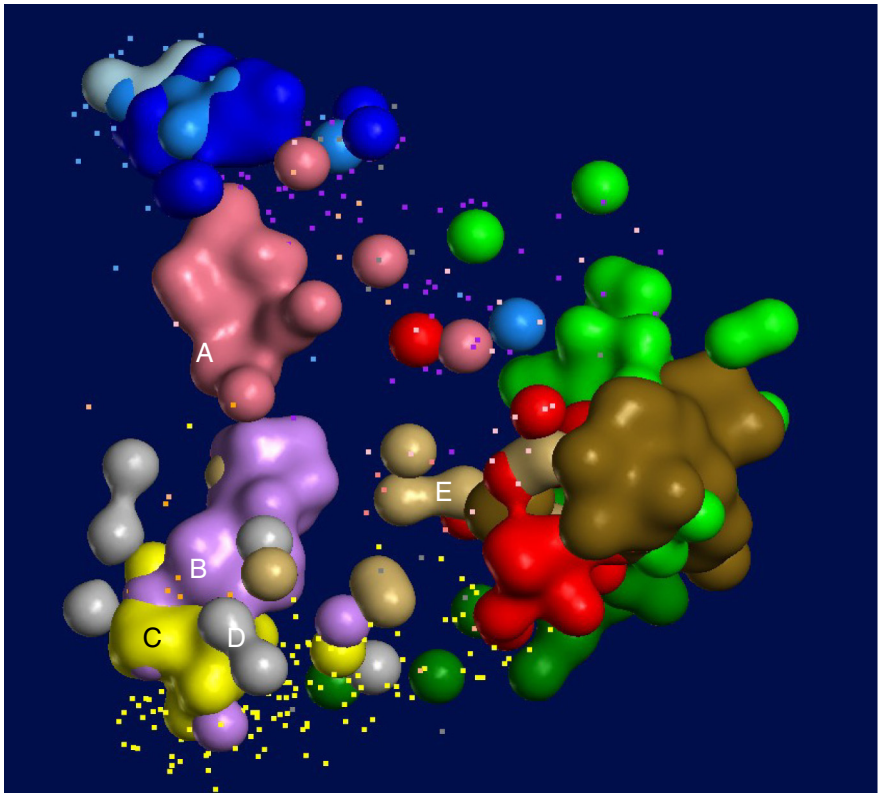

Fig. 18. View of epithermal sub-groups A–E in MDS1-MDS2-PC3 space. Wire-frames for MVT, VHMS, skarn, Sn-W, porphyry Mo, orogenic-Au and Carlin Au samples removed for clarity.

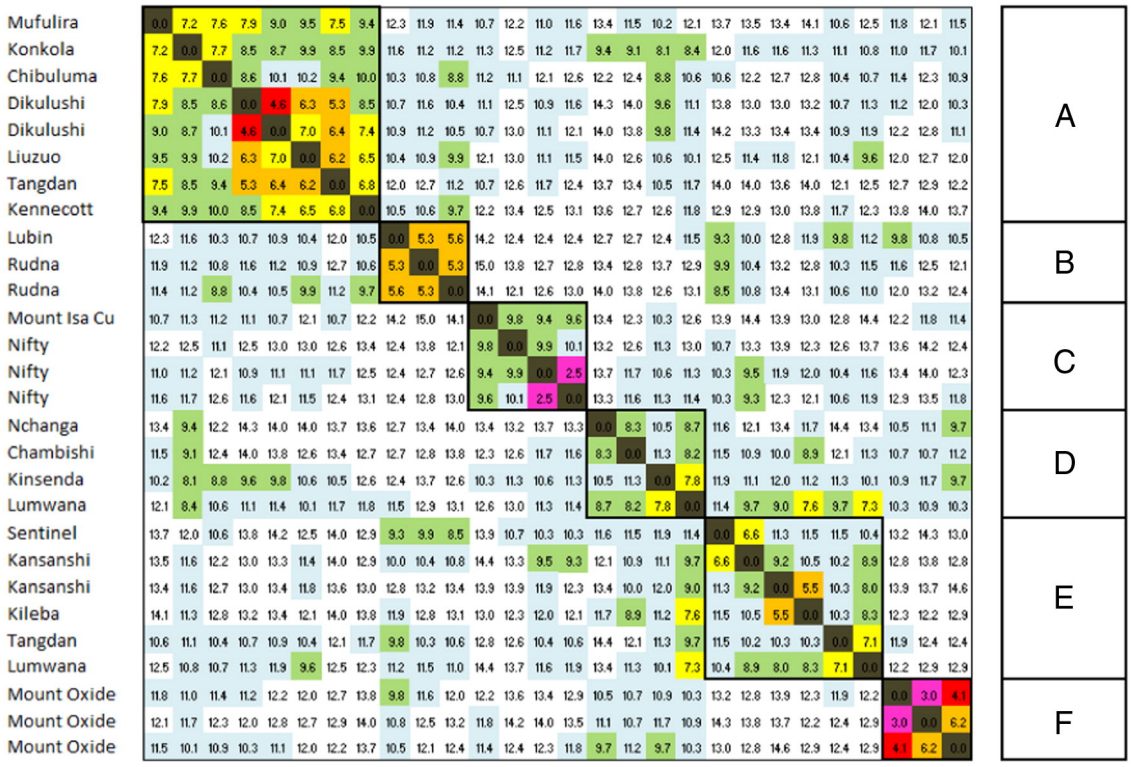

Fig. 19. Euclidean Distance Matrix for 28 sediment-hosted Cu samples arranged after Ward clustering routine. "Hottest" colours represent most proximal sample pairs with smallest Euclidean distance. (For interpretation of the references to colour in this figure legend, the reader is referred to the web version of this article.)

database. Geographically, much of the Pacific Rim is poorly represented in the database. As the OSNACA Project proceeds a more representative sample collection and database will be acquired.

Finally and most importantly, unless they are integrated with other geoscientific data, samples plotted in MH-Space only document inter-element ratios for 24 ore and pathfinder elements. They do not discriminate complex paragenetic histories. On its own, whole rock geochemistry does not definitively constrain the temperature and pressure of ore formation, nor the source of the ore fluids. Rather than interpreting ore genesis directly, a better way to use MH-Space is as a framework for raising further questions. If samples from different deposits have an unexpectedly close relationship in MH-Space, that my prompt a researcher to look for relationships between the deposits that have not been recognised before. Conversely, large distances between ore samples that are thought to be closely related will prompt a researcher to explain why.

7.2. Relationships between MH-Space and hydrothermal fluids

Relationships between different mineral systems and the nature of their hydrothermal fluids is a large and complex research field, but some general observations can be made in the context of reviews like Seward et al. (2013) and Wood and Samson (1998). Four major hydrothermal fluid types are plotted with respect to major ore deposit classes on the "main hydrothermal plane" in MH-Space (Fig. 26). The Zn to Cu-Au trend parallels a progression in ore deposit classes from those dominated by sedimentary basinal fluids, through modified seawater to those dominated by magmatic fluids. Typical ore fluid temperature rises along this trend. Sediment hosted Cu samples are the main anomaly in this scheme. Despite plotting close to other Cu-rich deposit samples, the ore fluids responsible for sediment hosted Cu deposits are widely regarded to be low-temperature basinal brines (e.g., Hitzman et al., 2010). The fourth major fluid type is a reduced, low-salinity CO_2-rich fluid that is widely reported in association with orogenic Au (e.g., Goldfarb et al., 2005). It is plotted at the Au-only end of the Cu-Au to Au-only trend where gold deposits formed from this type of fluid predominate (Fig. 26).

Minor, but important, contributions of magmatic fluids are commonly invoked for a variety of mineral systems where another ore fluid predominates. Examples include VHMS (e.g., Yang and Scott, 2005), orogenic-Au (e.g., Robert, 2001; Mueller, 2007; Bath et al., 2013; Vaughn and Ridley, 2014) and particularly epithermal (e.g., Hedenquist et al., 1998; Heinrich, 2005). The thick black arrows on Fig. 26 represent the evolution of magmatic fluids along their flow paths to compositions more like evolved seawater, metamorphic or basinal. Not shown on Fig. 26 is the spectrum of magmatic fluids associated with Cu-Au, Cu-Mo, Mo and Sn-W deposits. This spectrum parallels the ultramafic-granitoid trend (Fig. 8b).

This greatly simplified view of hydrothermal fluid compositions still explains much of the gross architecture of MH-Space. More subtle variations in hydrothermal fluid composition related to factors including pressure, the chemistry of sedimentary basin fill, volcanic pile composition and magma chemistry can be expected to correspond to more subtle variations in ore-element signatures.

8. Conclusions and further work

8.1. Conclusions

MH-Space is a mathematical construct which can be used to map variations in ore-element signature between samples. At the global scale, there are three important trends in MH-Space

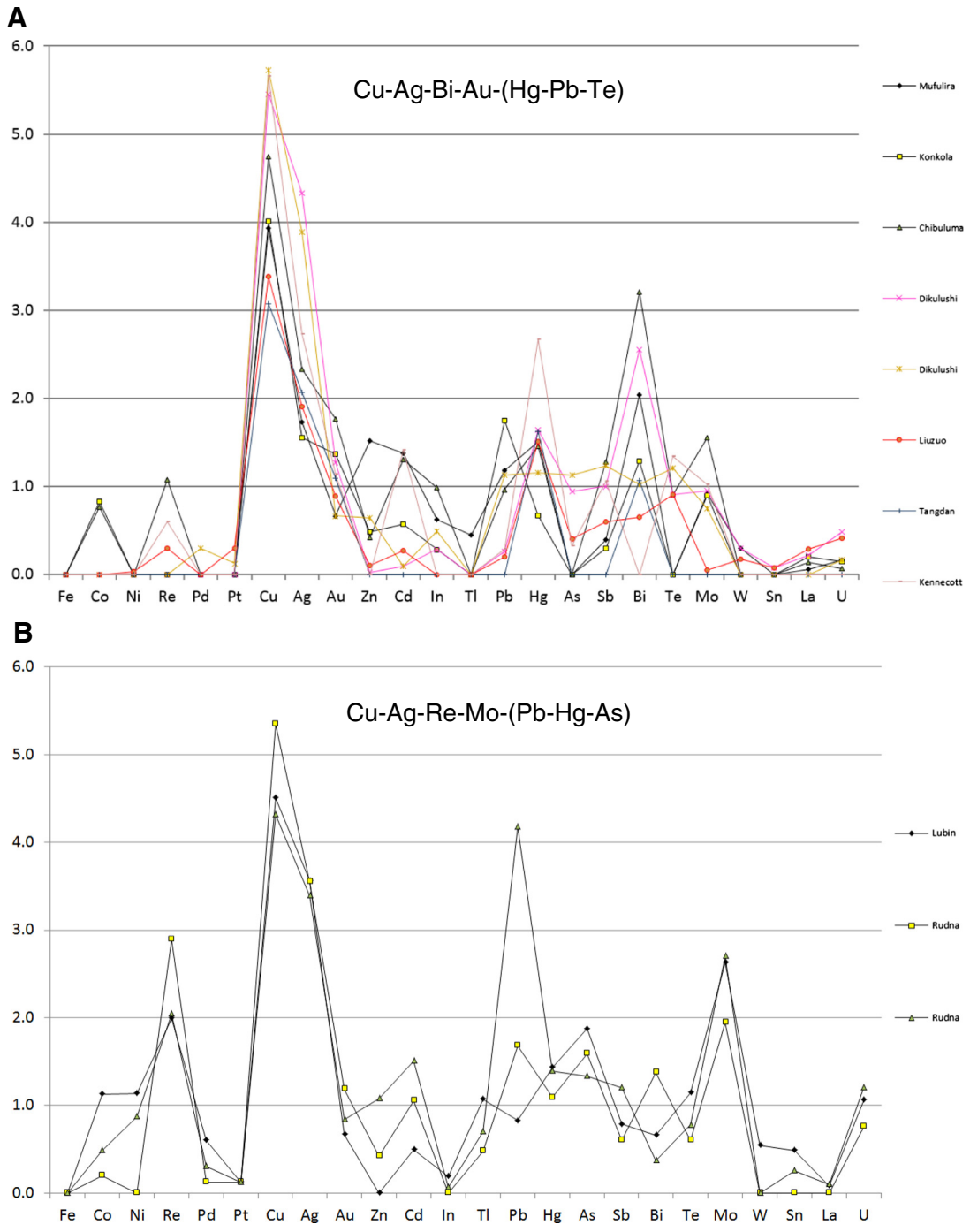

Fig. 20. Enrichment plots for sediment hosted Cu sub-groups A–F shown on Fig. 19.

1. Zn to Cu-Au,
2. Cu-Au to Au-only, and
3. Ni to Sn-W.

The "main hydrothermal plane" lies orthogonal to the Ni to Sn-W trend and contains the Zn to Cu-Au and Cu-Au to Au-only trends. Ore deposit classes overlap in MH-Space defining a geochemical continuum from MVT and SHMS deposits, through VHMS to Cu-Au rich classes like porphyry-Cu and IOCG. From the Cu-Au rich classes extends the orogenic-Au class to the Carlin-Au class. Most epithermal samples span the gap between the orogenic-Au and SHMS-VHMS classes. Magmatic Ni-Cu-PGE samples define a space separate to other deposit classes but some IOCG samples extend towards magmatic Ni-Cu-PGE space. Samples from granitoid-related deposits like porphyry Mo and Sn-W lie far from magmatic Ni-Cu-PGE samples on the other side of the "main hydrothermal plane".

More detailed mapping of sub-groups in the orogenic-Au, VHMS, epithermal and sediment hosted Cu classes refines our understanding of the geochemical continuum in MH-Space. Orogenic-Au deposits include different sub-groups of samples with geochemical

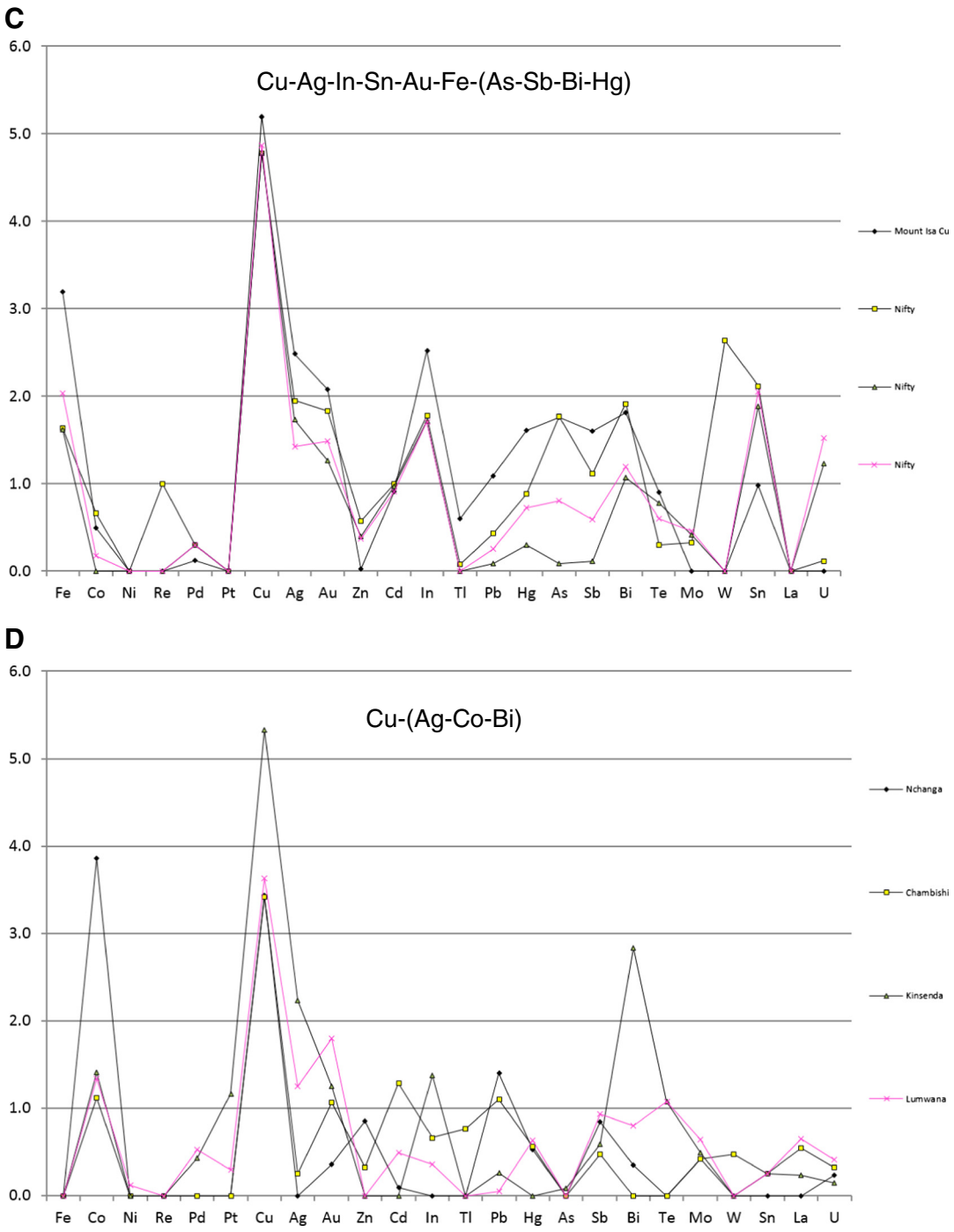

Fig. 20 (*continued*).

signatures transitional to porphyry-Cu, epithermal, Carlin Au and granitoid-related mineralisation. Zn-rich epithermal samples have signatures transitional to SHMS-VHMS samples, base-metal poor epithermal samples overlap with orogenic-Au and Carlin samples, whereas Cu-rich epithermal samples overlap with porphyry-Cu samples. Cu-rich VHMS samples overlap with Cu-Au rich classes like porphyry Cu, whereas Zn-Cu VHMS samples overlap with SHMS and epithermal samples.

8.2. Further work

Although the gross architecture of MH-Space appears to be well defined, there are several details that warrant further investigation, in addition to those listed above. In respect of the entire dataset, the analysis presented here is limited to a very superficial classifications of the data. The 16 major ore deposit classes were assumed at the beginning of the investigation. Sub-groups are defined by cluster

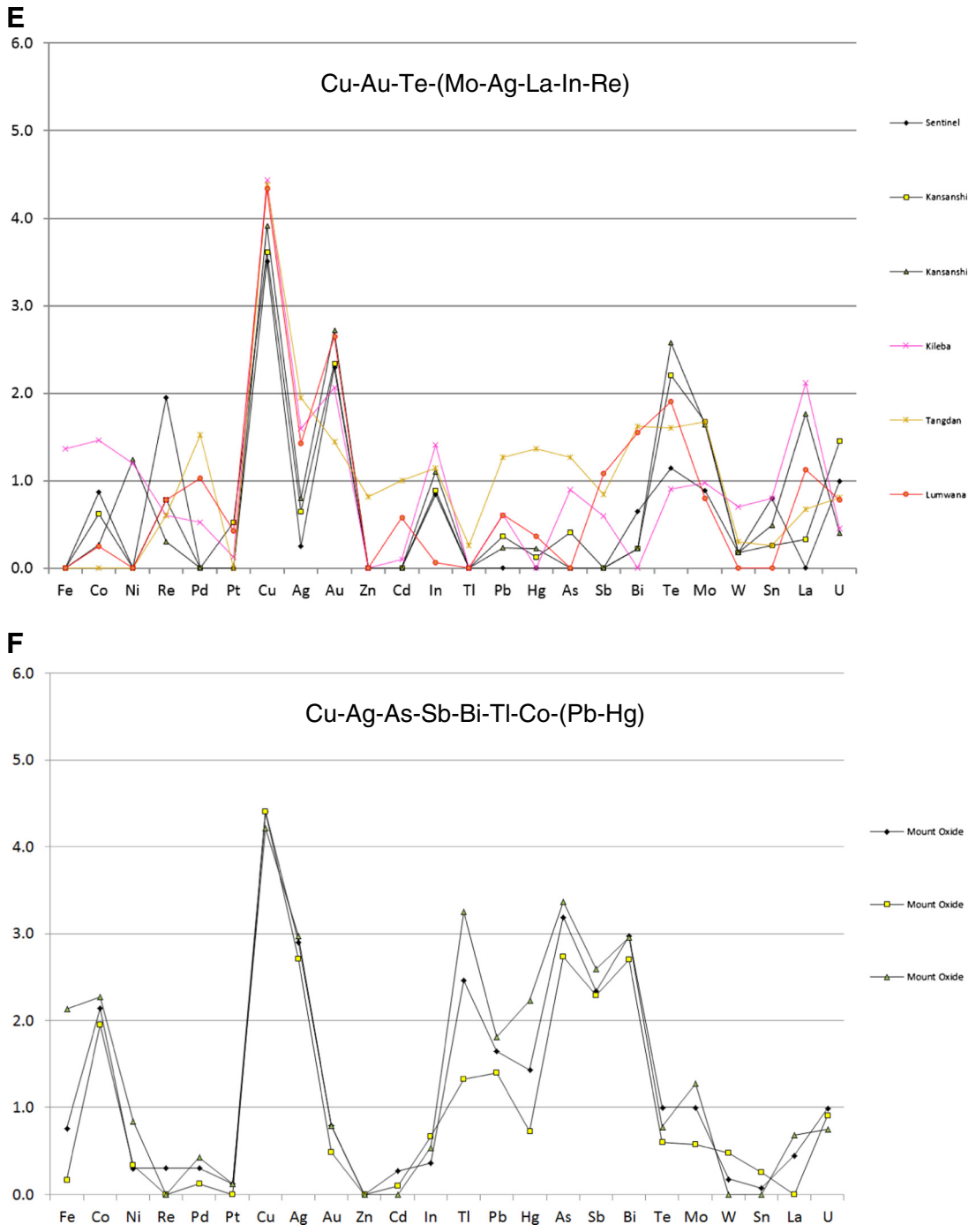

Fig. 20 (*continued*).

analysis within four of these ore-deposit classes but it is assumed that samples belong to their respective major classes to begin with. Supervised and unsupervised classification techniques such as self-organising maps will be useful to further explore MH-Space. It is hoped that further research on mathematical transforms will lead to better ways of presenting MH-Space. In particular, better methods of isolating variation owing to mineralisation from total variation in geochemical data will be of benefit. Most of the unwanted variation in the data is related to lithology and there may be better filters than censoring the data at ACA to remove this variation.

There are several unresolved problems in specific parts of MH-Space. Epithermal sub-group E overlaps the porphyry-Cu population. These are Cu-Au-Bi-Ag rich epithermal samples. However, most epithermal samples plot well away from Cu-Au ore deposit classes (Fig. 18). Is there are mineral-systems connection between epithermal sub-groups A-C and porphyry-Cu deposits? If there is, there is a very substantial modification of the metal signature across the porphyry-epithermal transition. Sampling mineralisation that could represent transitional material is one way of investigating the problem further.

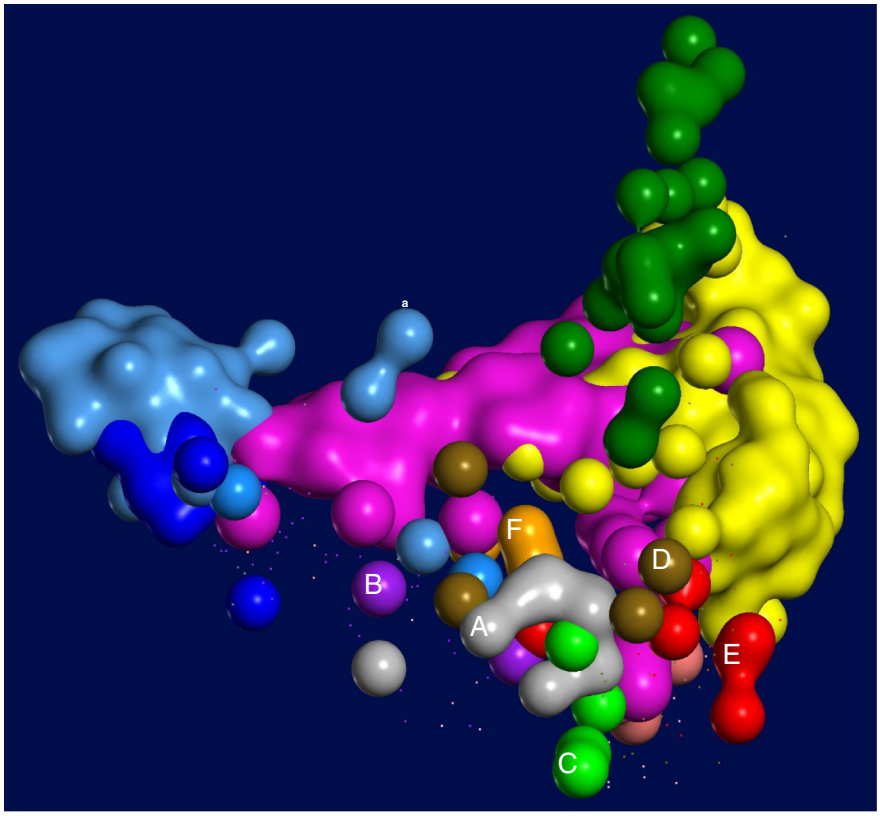

Fig. 21. View of sediment hosted Cu sub-groups A–F in MDS1-MDS2-PC3 space. Wire-frames for porphyry Cu, IOCG, VHMS, Sn-W and Carlin Au samples removed for clarity. Two MVT outliers labelled a. are two samples from Lisheen in Ireland with high Ni-Cu.

700181	0.0	10.3	11.9	10.9	10.9	12.2	9.1	9.2	9.6	9.7	11.1	13.6	10.9	12.6	12.1	12.8	12.2	13.7	14.0	A
700182	10.3	0.0	6.7	5.5	6.4	7.0	7.2	8.1	9.0	8.7	7.6	10.2	8.0	10.2	9.4	9.5	10.0	11.4	12.3	B
700187	11.9	6.7	0.0	4.4	6.2	5.8	9.1	10.8	10.8	10.5	10.2	9.8	9.6	9.7	11.2	10.0	11.0	11.6	11.5	
700189	10.9	5.5	4.4	0.0	6.2	6.5	9.8	10.2	10.2	10.4	10.5	10.1	9.5	10.8	10.2	10.1	10.5	12.0	12.5	
700188	10.9	6.4	6.2	6.2	0.0	7.5	7.4	8.4	9.1	9.8	9.6	8.3	6.3	10.0	9.8	10.4	11.0	11.5	12.1	
700183	12.2	7.0	5.8	6.5	7.5	0.0	9.2	9.7	11.1	9.6	10.0	7.7	8.9	8.1	8.8	7.6	8.6	9.8	9.5	
700184	9.1	7.2	9.1	9.8	7.4	9.2	0.0	4.3	6.1	5.5	6.0	10.0	5.9	9.0	9.0	9.1	9.5	10.2	11.2	C
700362	9.2	8.1	10.8	10.2	8.4	9.7	4.3	0.0	5.9	4.4	7.0	10.2	5.6	10.0	7.2	8.9	8.7	10.0	11.7	
700186	9.6	9.0	10.8	10.2	9.1	11.1	6.1	5.9	0.0	5.6	6.8	12.3	8.6	11.1	9.4	10.5	10.2	10.7	13.9	
700298	9.7	8.7	10.5	10.4	9.8	9.6	5.5	4.4	5.6	0.0	5.5	10.9	7.4	9.0	6.7	7.6	7.1	8.2	12.2	
700361	11.1	7.6	10.2	10.5	9.6	10.0	6.0	7.0	6.8	5.5	0.0	11.2	8.5	8.5	8.5	8.7	8.9	9.2	12.4	
700295	13.6	10.2	9.8	10.1	8.3	7.7	10.0	10.2	12.3	10.9	11.2	0.0	7.0	6.7	7.6	7.5	7.9	7.8	8.3	D
700296	10.9	8.0	9.6	9.5	6.3	8.9	5.9	5.6	8.6	7.4	8.5	7.0	0.0	9.1	7.4	8.9	8.9	9.4	10.8	
700363	12.6	10.2	9.7	10.8	10.0	8.1	9.0	10.0	11.1	9.0	8.5	6.7	9.1	0.0	8.3	6.3	6.9	6.5	7.7	
700297	12.1	9.4	11.2	10.2	9.8	8.8	9.0	7.2	9.4	6.7	8.5	7.6	7.4	8.3	0.0	5.4	3.9	6.0	11.0	
700357	12.8	9.5	10.0	10.1	10.4	7.6	9.1	8.9	10.5	7.6	8.7	7.5	8.9	6.3	5.4	0.0	3.4	4.4	8.8	
700359	12.2	10.0	11.0	10.5	11.0	8.6	9.5	8.7	10.2	7.1	8.9	7.9	8.9	6.9	3.9	3.4	0.0	4.6	10.1	
700360	13.7	11.4	11.6	12.0	11.5	9.8	10.2	10.0	10.7	8.2	9.2	7.8	9.4	6.5	6.0	4.4	4.6	0.0	9.0	
700358	14.0	12.3	11.5	12.5	12.1	9.5	11.2	11.7	13.9	12.2	12.4	8.3	10.8	7.7	11.0	8.8	10.1	9.0	0.0	

Fig. 22. Euclidean Distance Matrix for 19 samples from Lake Cowal deposit arranged after Average clustering routine. "Hottest" colours represent most proximal sample pairs with smallest Euclidean distance. (For interpretation of the references to colour in this figure legend, the reader is referred to the web version of this article.)

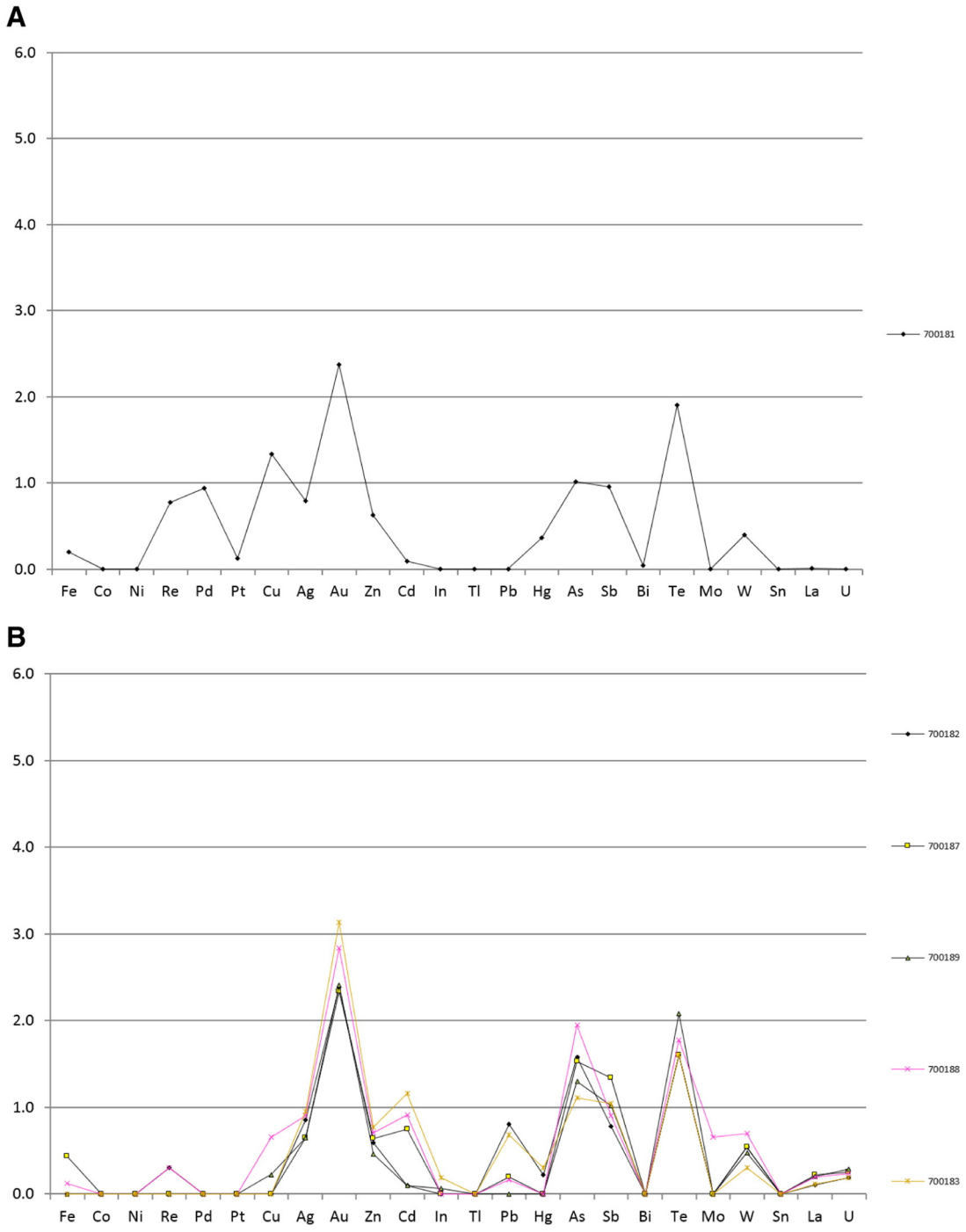

Fig. 23. Enrichment plots for Lake Cowal sub-groups A–D shown on Fig. 22.

Orogenic-Au samples, which includes samples from Intrusion Related Au deposits, have transitional geochemical relationships with epithermal, porphyry-Cu and Carlin Au classes. It will be of interest to compare the geological setting of deposits from these areas of overlap where different deposit classes have similar metal signatures. If a geochemical continuum can be established, can a broader geological continuum be established too?

The sediment hosted Cu class is too poorly sampled to properly unravel the complexities shown in Figs. 19–21. With a more comprehensive dataset for this class it will be possible to confirm whether Cu-Au-Mo-Te rich deposits (sub-group E) form a separate class to other sediment hosted Cu deposits. A better sense of intra-deposit variation in metal signature for a handful of sediment hosted Cu deposits will also make it easier to judge whether the divisions shown on Figs. 19–21 are sensible subdivisions for this ore deposit class.

The IOCG class has attracted much controversy with disagreement over which deposits to include (Groves et al., 2010). Once again, further sampling, particularly in areas of MH-Space that are transitional to other deposit classes will improve the definition of

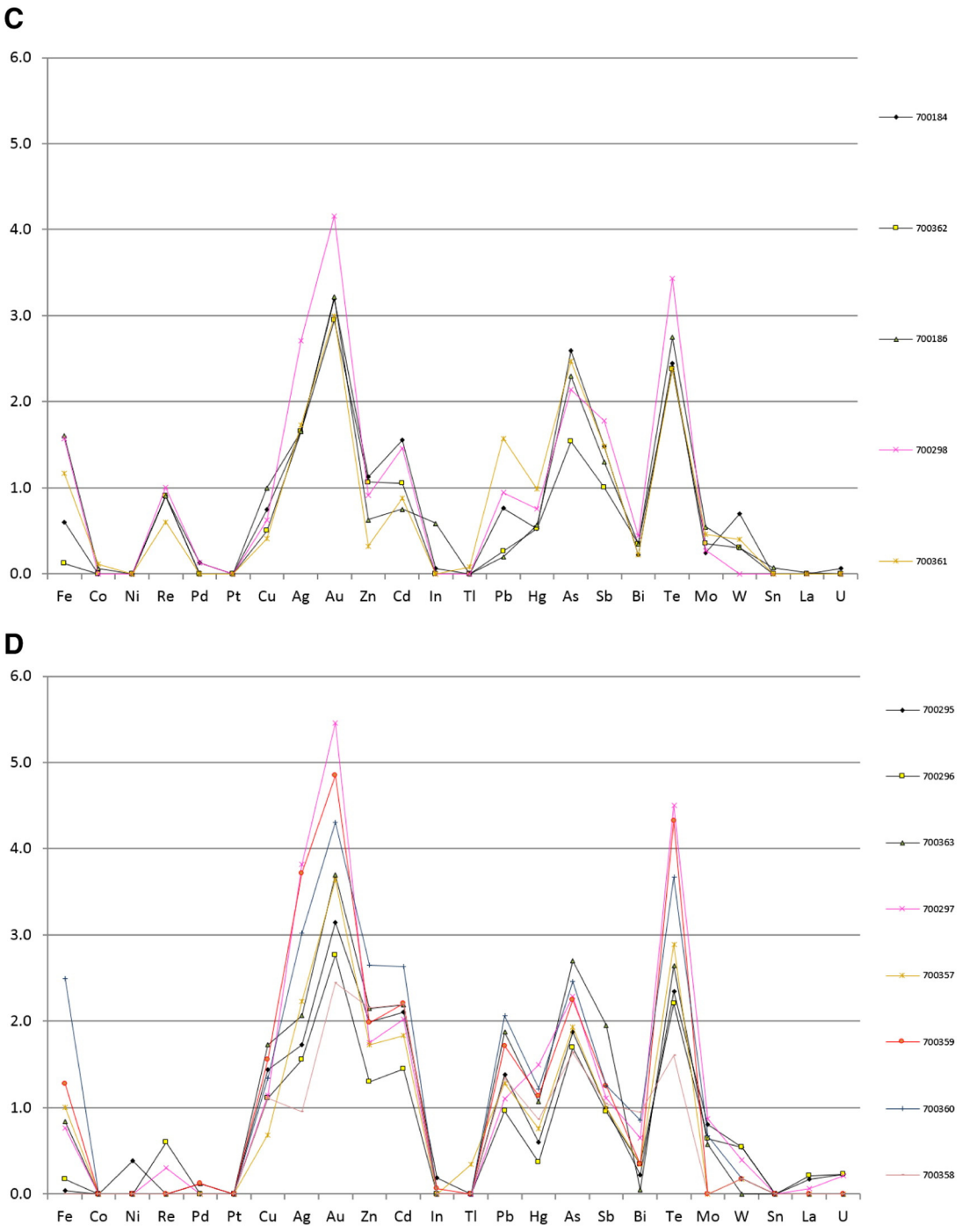

Fig. 23 (*continued*).

MH-Space and our understanding of the place of IOCG deposits within it.

Acknowledgements

Alex Christ and his team at Bureau Veritas – Ultratrace are warmly acknowledged for their tireless efforts in the laboratory and for their company's in-kind support. The OSNACA Project is entirely industry funded and would not have been possible without generous donations from Sipa Resources Limited, First Quantum Minerals Limited, Newmont Australia-Pacific, Sandfire Resources NL, Antofagasta Minerals, CSA Global, Integra Mining Limited, Wythenshawe Pty Ltd and Digirock. CWB particularly acknowledges financial and logistical support from Sipa Resources Limited. ECG is grateful for financial support provided by the Centre for Exploration Targeting (CET) at the University of Western Australia (UWA) and the Targeted Geoscience Initiative IV (TGI-4) from the Geological Survey of Canada, Natural Resources, Canada. SGH acknowledges support from the CET within the School of Earth and Environment, UWA. We thank the many people who have kindly donated ore samples to the OSNACA Project. Numerous high-

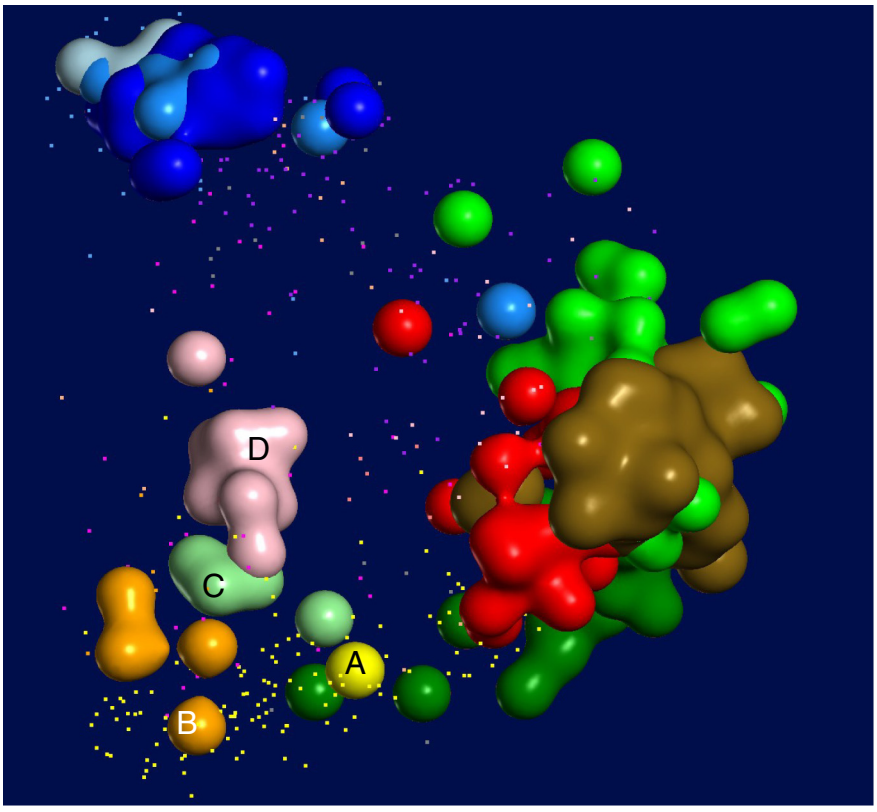

Fig. 24. Lake Cowal sub-groups A–D from same perspective of three-dimensional MH-Space as Fig. 18. Epithermal sub-groups removed for clarity.

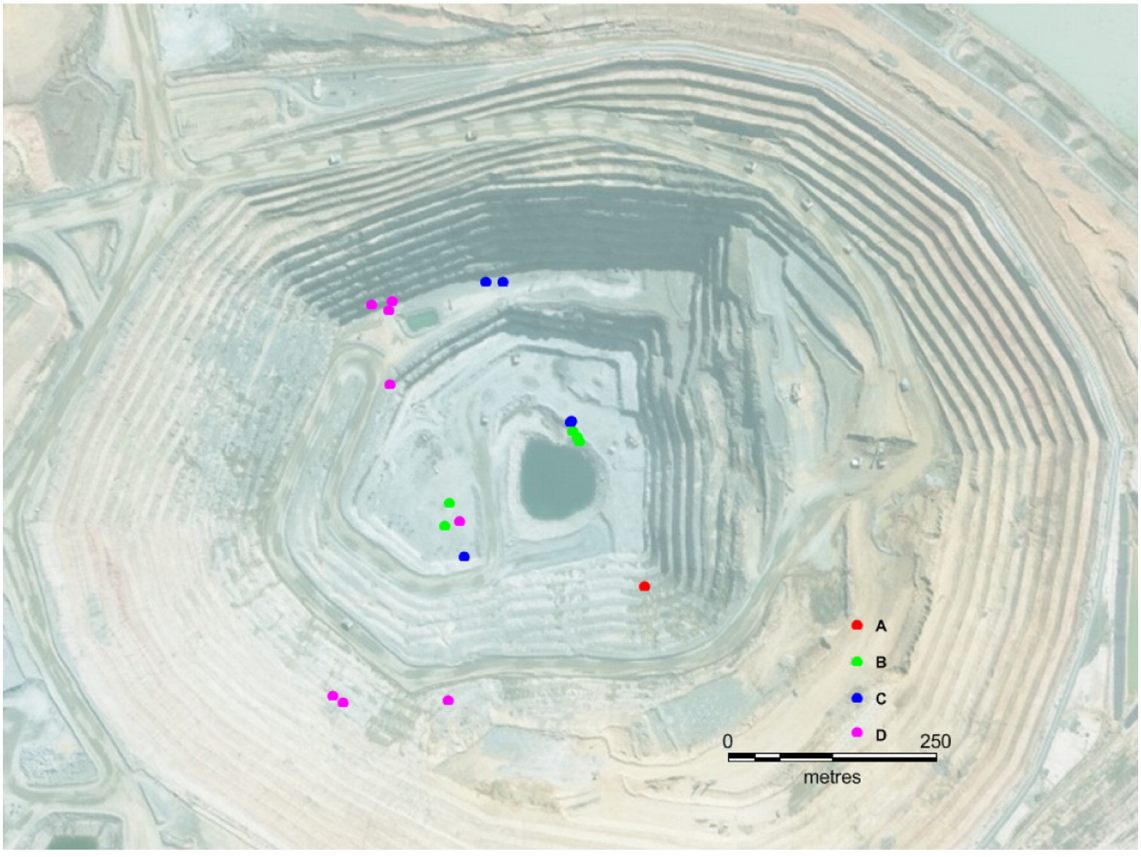

Fig. 25. Location of 19 Lake Cowal samples colour-coded by sub-group. Samples taken between −16 and 92 m RL. (For interpretation of the references to colour in this figure legend, the reader is referred to the web version of this article.)

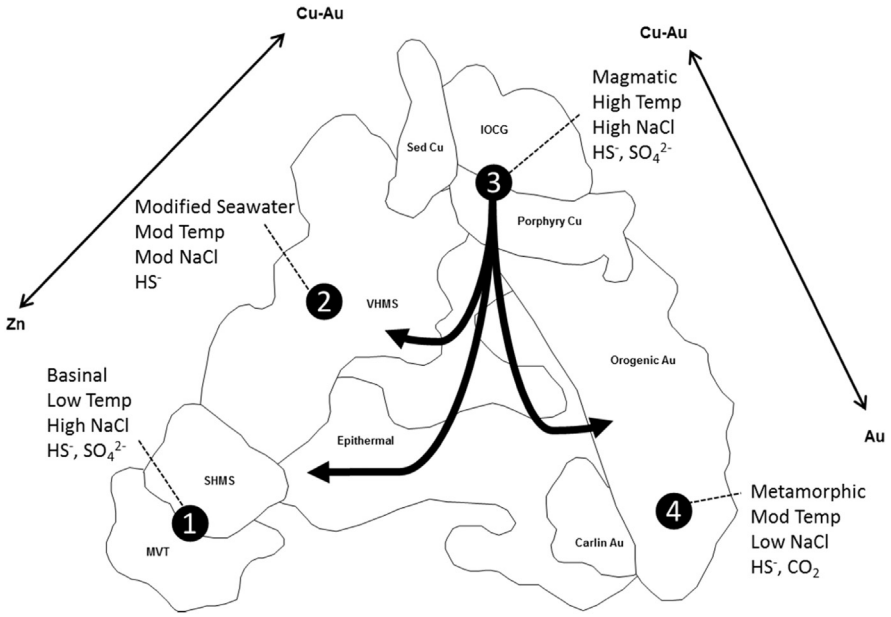

Fig. 26. Locations in MH-Space (view as for Fig. 8a) where four different hydrothermal fluid types predominate. Thick black arrows represent contributions of magmatic fluids into environments dominated by other fluids.

quality specimens were donated by the Geological Survey of Canada (Benoit Dube), Peter Muhling, Neal Reynolds, Graham Jeffress, Mark Allen, Bruce Hooper and the University of Tasmania (Ross Large).

References

Aitchison, J., 1986. The statistical analysis of compositional data. Monographs on Statistics and Applied Probability. Chapman & Hall Ltd., London (416 p).

Arribas Jr., A., Hedenquist, J.W., Itaya, T., Okada, T., Concepcion, R.A., Garcia Jr., J.S., 1995. Contemporaneous formation of adjacent porphyry and epithermal Cu-Au deposits over 300 Ka in northern Luzon, Philippines. Geology 23, 337–340.

Bath, A.B., Walshe, J.L., Cloutier, J., Verrall, M., Cleverley, J.S., Pownceby, M.I., Macrae, C.M., Wilson, N.C., Tunjic, J., Nortje, G.S., Robinson, P., 2013. Biotite and apatite as tools for tracking pathways of oxidized fluids in the Archean east repulse gold deposit, Australia. Econ. Geol. 108, 667–690.

Fernández, A., Gómez, S., 2008. Solving non-uniqueness in agglomerative hierarchical clustering using multidendrograms. J. Classif. 25, 43–65.

Goldfarb, R.J., Baker, T., Dube, B., Groves, D.I., Hart, C.J.R., Gosselin, P., 2005. Distribution, character, and genesis of gold deposits in metamorphic terranes. In: Hedenquist, J.W., Thompson, J.F.H., Goldfarb, R.J., Richards, J.P. (Eds.), Economic Geology. 100th Anniversary Volume 1905–2005, pp. 407–450.

Groves, D.I., Bierlein, F.P., Meinert, L.D., Hitzman, M.W., 2010. Iron oxide copper-gold (IOCG) deposits through Earth history: implications for origin, lithospheric setting, and distinction from other epigenetic iron oxide deposits. Econ. Geol. 105, 641–654.

Hannington, M.D., Poulsen, K.H., Thompson, J.F.H., Sillitoe, R.H., 1999. Volcanogenic gold in the massive sulfide environment. In: Barrie, C.T., Hannington, M.D. (Eds.), Volcanic-associated Massive Sulfide Deposits: Processes and Examples in Modern and Ancient Settings: Reviews in Economic Geology. 8, pp. 325–356.

Hedenquist, J.W., Thompson, J.F.H., Goldfarb, R.J., Richards, J.R. (Eds.), 2005. Economic Geology One Hundredth Anniversary Volume 1905–2005 (1136 p).

Hedenquist, J.W., Arribas Jr., A., Reynolds, T.J., 1998. Evolution of an intrusion-centered hydrothermal system: Far Southeast-Lepanto porphyry and epithermal Cu-Au deposits, Philippines. Econ. Geol. 93, 373–404.

Heinrich, C.A., 2005. The physical and chemical evolution of low salinity magmatic fluids at the porphyry to epithermal transition: a thermodynamic study. Mineral. Deposita 39, 864–889.

Hitzman, M.W., Selley, D., Bull, S., 2010. Formation of sediment-hosted stratiform copper deposits through Earth history. Econ. Geol. 105, 627–640.

Leach, D.L., Sangster, D.F., Kelley, K.D., Large, R.R., Garven, G., Allen, C.R., Gutzmer, J., Walters, S.G., 2005. Sediment-hosted lead-zinc deposits: a global perspective. In: Hedenquist, J.W., Thompson, J.F.H., Goldfarb, R.J., Richards, J.P. (Eds.), Economic Geology, 100th Anniversary Volume, pp. 561–607.

Lindgren, W., 1913. Mineral Deposits. McGraw-Hill Book Company, New York (883 p).

Longerich, H.P., Jenner, G.A., Freyer, B.J., Jackson, S.E., 1990. Inductively coupled plasma - mass spectrometric analysis of geological samples: a critical evaluation based on case studies. Chem. Geol. 83, 105–118.

Lydon, J.W., 1984. Ore deposit models; 8, volcanogenic sulfide deposits; part I: a descriptive model. Canada]–>Geosci. Can. 11, 195–202.

Mortensen, J.K., Craw, D., MacKenzie, D.J., Gabites, J.E., Ullrich, T., 2010. Age and origin of orogenic gold mineralization in the Otago Schist belt, South Island, New Zealand: Constraints from lead isotope and $^{40}Ar/^{39}Ar$ dating studies. Econ. Geol. 105, 777–793.

Mueller, A.G., 2007. Copper-gold endoskarns and high-Mg monzodiorite-tonalite intrusions at Mt. Shea, Kalgoorlie, Australia: implications for the origin of gold-pyrite-tennantite mineralization in the Golden Mile. Mineral. Deposita 42, 737–769.

Nesbitt, B.E., 1988. Gold deposit continuum: a genetic model for lode Au mineralization in the continental crust. Geology 16, 1044–1048.

OSNACA, 2015. OSNACA: Ore samples normalised to average crustal abundance. http://www.cet.edu.au/research-projects/special-projects/projects/osnaca-ore-samples-normalised-to-average-crustal-abundance (November 2015).

Robert, F., 2001. Syenite-associated disseminated gold deposits in the Abitibi greenstone belt, Canada. Mineral. Deposita 36, 503–516.

Rudnick, R.L., Gao, S., 2003. The composition of the continental crust. In: Rudnick, R.L., Holland, H.D., Turekian, K.K. (Eds.), The Crust, Vol. 3, Treatise on Geochemistry. Elsevier-Pergamon, Oxford, pp. 1–64.

Seward, T.M., Williams-Jones, A.E., Migdisov, A.A., 2013. The chemistry of metal transport and deposition by ore-forming hydrothermal fluids. Treatise on Geochemistry, Second edition Elsevier Science, pp. 29–57.

Vaughn, E.S., Ridley, J.R., 2014. Evidence for exsolution of Au-ore fluids from granites crystallized in the mid-crust, Archaean Louis Lake Batholith, Wyoming. London, Special Publications]–>Geol. Soc. Lond., Spec. Publ. 402, 103–120.

Wood, S.A., Samson, I.M., 1998. Solubility of ore minerals and complexation of ore metals in hydrothermal solutions. In: Richards, J.P., Larson, P. (Eds.), Techniques in Hydrothermal Ore Deposit Geology, Reviews in Economic Geology v.10. Society of Economic Geologists, pp. 33–80 (Ch. 2).

Yang, K., Scott, S.D., 2005. Magmatic sources of volatiles and base metals for volcanogenic massive sulfide deposits on modern and ancient seafloors: evidence from melt inclusions. In: J., M., Berlein, F.P. (Eds.), Mineral Deposits Research: Meeting the Global Challenge. Springer, pp. 715–718.